Sedimentary anatomy and hydrological record of relic fluvial deposits in a karst cave conduit

PAVEL BELLA*,†, MICHAŁ GRADZIŃSKI‡, HELENA HERCMAN§, STANISŁAW LESZCZYŃSKI‡ and WOJCIECH NEMEC¶ (iD)

*State Nature Conservancy of the Slovak Republic, Slovak Caves Administration, 031 01 Liptovský Mikuláš, Slovak Republic
†Department of Geography, Pedagogical Faculty, Catholic University in Ružomberok, 034 01 Ružomberok, Slovak Republic
‡Institute of Geological Sciences, Jagiellonian University, 30-387 Kraków, Poland
§Institute of Geological Sciences, Polish Academy of Sciences, 00-818 Warszawa, Poland
¶Department of Earth Science, University of Bergen, 5007 Bergen, Norway
(E-mail: wojtek.nemec@uib.no)

Associate Editor – Nick Eyles

ABSTRACT

This case study from the renowned Demänová Cave System in the Carpathians of Slovakia demonstrates that the conventional methods of fluvial sedimentology, combined with an allostratigraphic mapping and speleothem U-series isotopic dating, can give unprecedented insights into the hydrological history of underground karst conduit. The deposits studied are a relic compound sidebar ranging from gravel to mud and encapsulating the conduit's hydrological history from the middle Pleistocene to the present time. A succession of 10 allostratigraphic units, time-constrained by speleothems, are recognized in the sidebar deposits, and the corresponding morphodynamics of an evolving cave-floor sedimentation are reconstructed in considerable detail. The subterranean river water stages recognized from the deposits, time-constrained by flowstone layers and stalagmites, correlate with and add to the regional record of climate changes. Two distinct episodes of flow ponding (high-stage slackwater conditions) are recognized and attributed to the independently documented downstream cave-roof collapses, probably triggered by the Carpathian post-orogenic earthquakes. This multidisciplinary study may serve as a useful methodological guide for the analysis of fluviokarstic deposits in speleological research and reconstruction of their hosting cave hydrological history.

Keywords Allogenic karst, compound sidebar, Demänová Cave System, Slovakia, speleothems, underground river, U-series isotope dating.

INTRODUCTION

Karst cave sediments have long attracted research as the underground depositories of plant and animal remains and as the archives of early human activity (e.g. Molodkov, 2001; Goldberg & Sherwood, 2006; Harmon & Wicks, 2006; Barton & Northup, 2007; Bird *et al.*, 2007; Shang *et al.*, 2007; Backwell *et al.*, 2008; Jass & George, 2010; Oliveira *et al.*, 2011; Pickering *et al.*, 2011; Wu *et al.*, 2012; Martini *et al.*, 2018). With the advent of high-precision mass-spectrometric U-series isotopic dating (Li *et al.*, 1989), the cave speleothems have become extensively studied to

Authors in alphabetical order.

reconstruct regional climate changes and land relief evolution, and to recognize and date the underground record of ancient earthquakes (e.g. Hercman, 2000; Kagan *et al.*, 2005; Haeuselmann *et al.*, 2007; Pickering *et al.*, 2007; Kicińska *et al.*, 2017; Polyak *et al.*, 2018). Speleologists have long advocated that the cave-fill clastic deposits are of crucial importance to a karst system history and require detailed sedimentological research (White & White, 1968; Stein, 1987; Harmon & Wicks, 2006; Sasowsky, 2007; White, 2007; Herman *et al.*, 2012). However, only a handful of such case studies have thus far been attempted worldwide, with a varied analytical insight (Quinif & Maire, 1998; Bosch & White, 2004; Knapp *et al.*, 2004; Kadlec *et al.*, 2008; Zupan Hajna *et al.*, 2008; Auler *et al.*, 2009; Ghinassi *et al.*, 2009; Martini, 2011; Kicińska *et al.*, 2017).

Particularly little sedimentological research has focused on cave clastic deposits to reconstruct the hydrological history of karst cave conduits, where the subterranean rivers are constrained by bedrock morphology and are no longer free to operate in their 'normal' manner known from the land-surface alluvial plains. Instead, their behaviour in cave conduits resembles that of rivers in bedrock mountain ravines (Tinkler & Wohl, 1998; Herman *et al.*, 2012). However, these conditions also mean that the river entire hydrological history is confined to and potentially recorded in a single narrow subterranean conduit.

Reconstruction of the hydrological history of underground conduits is crucial to palaeoclimate studies and to the landscape evolution in karstic terranes, as the subterranean drainage limits surface water and may allow few or no surficial rivers or lakes to form, or can make such land-surface features virtually disappear. Many land areas in the world are karstic terranes (Assaad & Jordan, 1994), which renders their hydrological systems highly vulnerable to the impending modern global climate change.

Fluvial deposits in cave conduits are sparsely preserved, but even their local relics can shed important light on the hydrological history of underground river conduits – as is demonstrated by the present case study from the Demänová Cave System of Slovakia. The study employs conventional sedimentological methods, combined with allostratigraphic outcrop mapping and speleothem U-series isotopic dating, to reconstruct in detail the hydrological history of the cave conduit and its changing internal morphodynamics of sediment accumulation and erosion from >350 ka to the present time. The deposits studied are a relic compound sidebar of the subterranean branch of the Demänovka River but are highly informative as a condensed local sedimentary hydrological record. Apart from its regional significance for the history of the Demänová Cave System, this case study may serve as a useful method guide for the sedimentological and hydrological analysis of fluviokarstic deposits in speleological research.

SPELEOLOGICAL SETTING

The Demänová Cave System (DCS), known as the Demänovský jaskynný systém in Slovak, is located in the north-trending Demänová Valley of the Slovakian Low Tatra Mountains of the Carpathian orogenic belt (Fig. 1). Glacial tills indicate that the upper part of the Demänová Valley was glaciated at least twice during the Pleistocene (Vitásek, 1923; Louček *et al.*, 1960; Droppa, 1972). The cave system formed in the Anisian–Ladinian carbonate rocks thrust by the Carpathian (Alpine) tectonism as a nappe over the granitoid crystalline core of the Low Tatra Mountains (Droppa, 1957; Bella *et al.*, 2014a; Gaál, 2016; Gaál & Michalík, 2017). The DCS is a renowned case of a multilevel karstic system formed by allogenic rivers and featured in many speleological textbooks (e.g. Sweeting, 1973; Warwick, 1976; Bögli, 1980; Jennings, 1985; Palmer, 2007). The cave system has a total length in excess of 41 km and includes 11 caves interconnected by looped conduits, distributed over a subsurface depth range of more than 190 m (Fig. 2; Herich, 2017).

Droppa (1966, 1972) distinguished nine cave levels in the DCS and correlated them with the surficial fluvial terraces of the Demänovka River and adjacent Váh River in the Liptov Basin. However, it remains disputed whether these cave levels represent the surficial water drainage table or rather a combination of the water table and phreatic adjustments (Bella, 1993; Bella *et al.*, 2014b). Droppa (1966, 1972) assigned tentatively the cave levels, long abandoned by fluviokarstic drainage, to the successive glacial stages of the classic Alpine morphostratigraphic scheme, but the U-series isotope dating subsequently revealed that they were actually older than presumed (Hercman *et al.*, 1997; Bella *et al.*, 2014b).
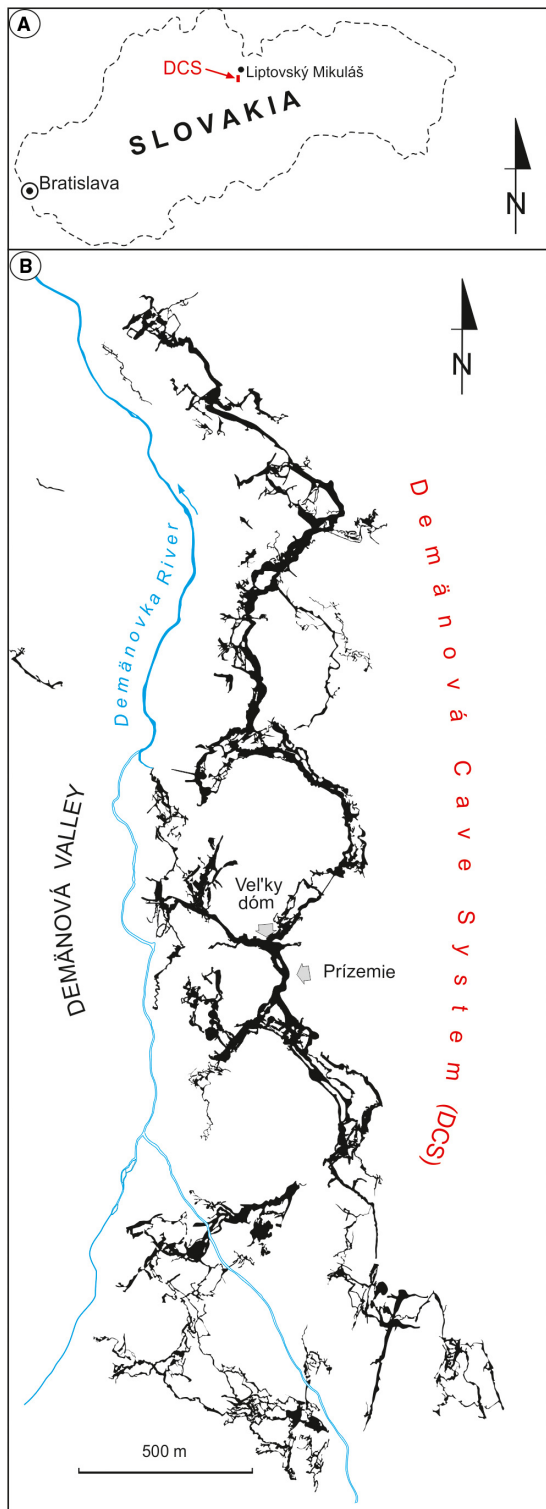
Fig. 1. (A) Location map of the Demänová Cave System (DCS) in northern Slovakia. (B) Plan-view extent of the DCS (modified from Herich, 2017) relative to the present-day surface flow route of the Demänovka River; note the location of the Prízemie and Veľký Dóm segments of the DCS conduit referred to in the text.

The present study is from the DCS level still active as a subterranean branch of the modern Demänovka River (Fig. 2) and dating to the middle Pleistocene until Holocene. Relics of cave fluvial deposits have been reported from the DCS (Droppa, 1957; Kojdová & Slíva, 2005), but the present study is the first attempt to decipher the hydrological history and morphodynamic sedimentation pattern of the underground cave system in its latest, post-early Pleistocene conduit (Fig. 2).

METHODS AND TERMINOLOGY

The study uses conventional sedimentological field methods, such as a detailed logging, measuring of bedding attitude and palaeocurrent directions, photographic documentation and a line drawing of bedding architecture on an outcrop photomosaic. Special attention is given to mappable outcrop-scale bedding discontinuities. The descriptive sedimentological terminology, including clast fabric notation, is according to Harms *et al.* (1975, 1982) and Collinson *et al.* (2006). The concept of allostratigraphic analysis is after NACSN (1983), with an allostratigraphic unit defined as a mappable sedimentary body bounded by bedding discontinuities. Such units represent the main increments of local sediment accumulation.

The U-series dating of speleothems, including chemical separation of uranium and thorium by the chromatographic method with TRU-Resin (Hellstrom, 2003), was conducted at the U-series Laboratory of the Institute of Geological Sciences of the Polish Academy of Sciences in Warsaw. Two different measurement methods were used: mass spectrometry and alpha spectrometry. The samples for mass spectrometry were between 0.1 g and 0.5 g. Mixtures of $^{233}U/^{236}U/^{229}Th$, calibrated by uraninite analysis in secular equilibrium, were used as a chemical procedure and isotopic fractionation control. The isotopic composition of U and Th was measured at the Institute of Geology of the Czech Academy of Sciences in Prague, using a double-focusing sector-field ICP mass analyzer (Element 2, Thermo Finnigan MAT; Thermo Fisher Scientific, Waltham, MA, USA).

The samples for alpha spectrometry were 0.5 to 2.0 g (mainly <1 g). Uranium and thorium were separated by a standard chemical procedure for carbonate samples (Ivanovich & Harmon, 1992), using a chromatographic method
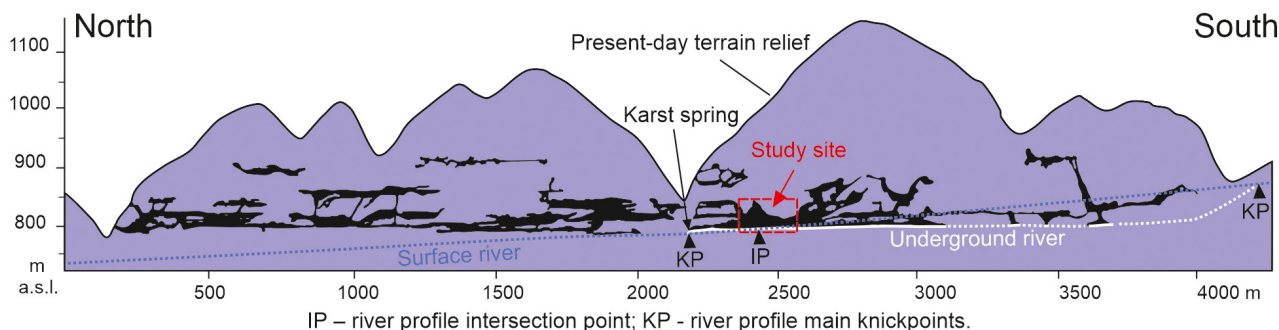
Fig. 2. Longitudinal vertical cross-section of the Demänová Cave System (DCS) (modified from Droppa, 1966, 1972), showing location of the studied Prízemie–Veľký Dóm segment of its lowest underground conduit. Note the projected level of the present-day surface route of the Demänovka River (cf. Fig. 1B).

with the DOWEX 1×8 ion exchanger (Sigma Aldrich, St. Louis, MO, USA). The chemical separation efficiency was controlled by the addition of a ^{228}Th/^{232}U spike (UDP10030 tracer solution by Isotrac, AEA Technology QSA, Carlsbad, CA, USA) before chemical treatment. The activity measurements were obtained on an Alpha Ensemble spectrometer (EG&G ORTEC/AMETEK, Oak Ridge, TN, USA) with 1200 mm^2 active area and ultra-low background detectors.

The U-series ages were calculated iteratively from the ^{230}Th/^{234}U and ^{234}U/^{238}U activity ratios, and are given herein with an error limit of two standard deviations, which means a confidence level of at least 95.4% (Table 1). The decay constants of Jaffey *et al.* (1971) for ^{238}U, Cheng *et al.* (2013) for ^{234}U and ^{230}Th, and Holden (1990) for ^{232}Th were used. Age errors do not include uncertainties related to the decay constants. Corrected ages were adjusted for detrital contamination indicated by the presence of ^{232}Th using the typical silicate activity ratio ^{230}Th/^{232}Th of 0.83 ($\pm$0.42) derived from the ^{232}Th/^{238}U activity ratio of 1.21 ($\pm$0.6), ^{230}Th/^{238}U activity ratio of 1.0 ($\pm$0.1) and ^{234}U/^{238}U activity ratio of 1.0 ($\pm$0.1) (cf. Cruz *et al.*, 2005). The initial value of the ^{234}U/^{238}U activity ratio (Table 1) was calculated based on the corrected activity ratio and sample age.

STUDY RESULTS

The deposits studied are preserved at the right-hand (eastern) margin of the modern subterranean branch of the Demänovka River in the Prízemie segment of the Demänovská Jaskyňa Slobody Cave (Figs 3 and 4A). The deposits have a thickness of around 4 m and a lateral extent of a few tens of metres, including their hanging upstream relics plastered on the cave wall (Fig. 3, upper right). Despite the limited extent of their outcrop, these relic deposits – interspersed with carbonate speleothems – encapsulate the hydrological and sedimentation history of the host cave conduit since the middle Pleistocene. The present study focuses on the allostratigraphy and sedimentological characteristics of these cave-side deposits, and on their hydrological and regional climatic implications.
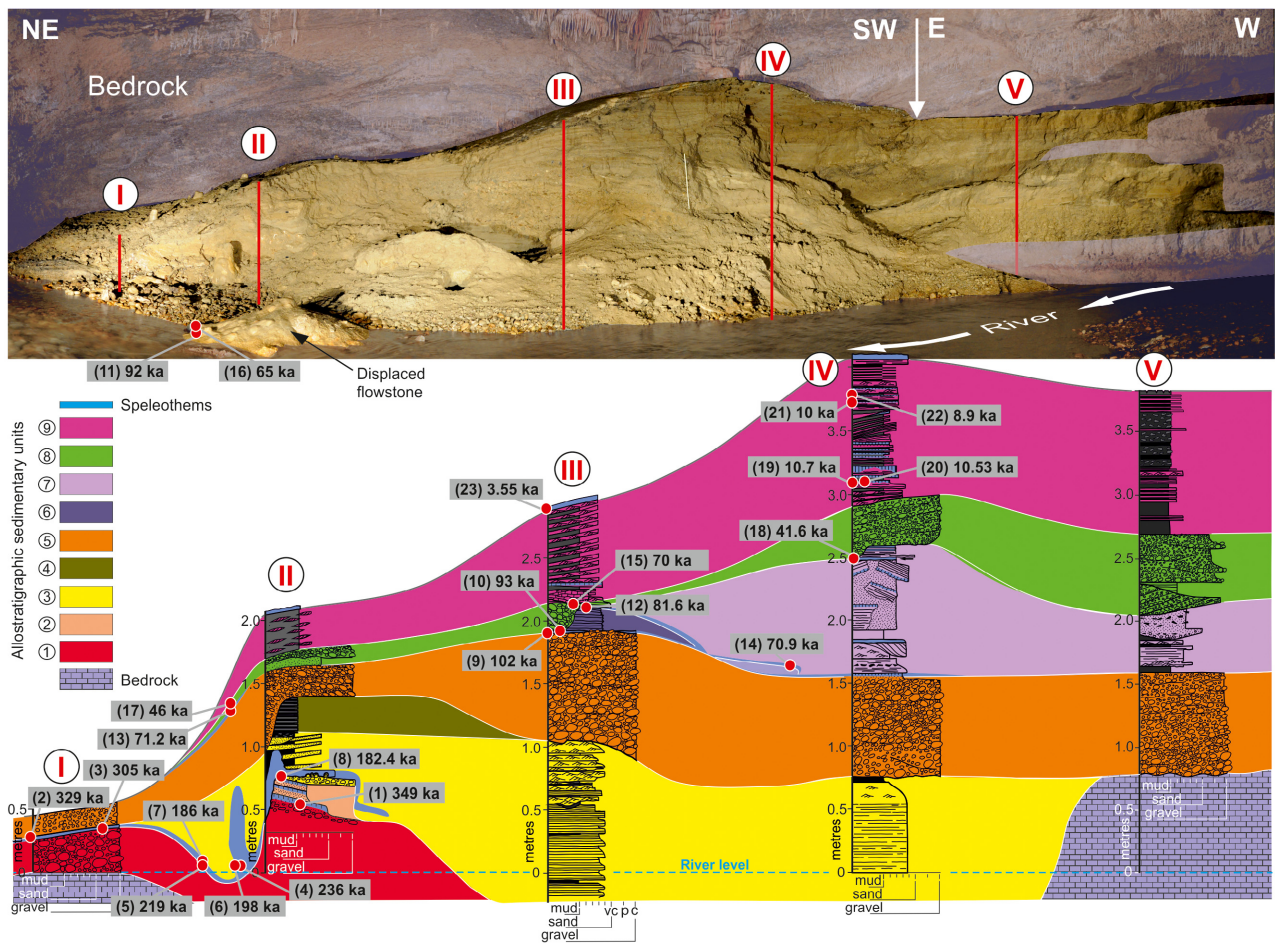
Allostratigraphic units

The cave-side deposits studied comprise alternating gravel, sand and mud (Fig. 4B). The sand and mud are siliciclastic, whereas gravel consists of both granitoid and carbonate rock clasts. The clastic deposits include intervening flowstone layers of various thickness and lateral extent, which were dated by the U-series isotopic method (Fig. 3, Table 1). The stacking pattern of deposits was recognized by allostratigraphic mapping of outcrop-scale discontinuities (Fig. 3) and detailed sedimentological analysis (Fig. 4B). The discontinuities are erosional unconformities with a variable relief and related facies changes, bounding ten allostratigraphic units. Nine of the units stand perched in the outcrop wall above the present-day river level (Fig. 3), whereas the youngest, tenth unit are deposits of the modern incised river floor. The following two sections of the text give sedimentological description and morphodynamic interpretation of the consecutive allostratigraphic units.

Table 1. U-series dating results of speleothem samples from the Prízemie and Veľký Dóm segment of the Demänová Cave System (see sample locations in Figs 3, 5 and 9). AR – activities ratio; sample number in bold – mass spectrometry analysis.

| Sample number	Sample lab. label	^{238}U (ppm)	^{234}U/^{238}U AR	^{230}Th/^{234}U AR	^{230}Th/^{232}Th AR	Age (ka)	Corrected age (ka)	Initial ^{234}U/^{238}U AR
	Prízemie cave passage							
1	RA 105.4	5.00 ± 0.03	0.889 ± 0.001	0.919 ± 0.002	145.6 ± 0.4	354 ± 6	349 ± 9	0.70 ± 0.01
2	RA 110	10.07 ± 0.05	0.957 ± 0.001	0.936 ± 0.003	50003 ± 26	329 ± 7	–	0.89 ± 0.02
3	RA 34/1	8.19 ± 0.04	0.888 ± 0.001	0.901 ± 0.002	1988 ± 7	305 ± 5	–	0.74 ± 0.01
4	RA 4 centre	5.10 ± 0.10	0.8990 ± 0.0123	0.8605 ± 0.0125	>1000	236 ± 10	–	0.80 ± 0.04
5	RA 3 bottom	8.30 ± 0.30	0.8806 ± 0.0149	0.8383 ± 0.0154	888 ± 359	219^{+11}_{-10}	–	0.78 ± 0.04
6	RA 4 side	4.21 ± 0.06	0.8807 ± 0.0097	0.8120 ± 0.0097	128 ± 13	198 ± 6	–	0.79 ± 0.03
7	RA 3 top	11.60 ± 0.30	0.9143 ± 0.0117	0.8030 ± 0.0111	21 ± 1	186 ± 6	–	0.86 ± 0.03
8	RA 105.1	9.61 ± 0.05	1.033 ± 0.001	0.816 ± 0.001	222406 ± 419	182.4 ± 0.4	–	1.055 ± 0.003
9	RA 106/1	8.14 ± 0.05	0.824 ± 0.001	0.594 ± 0.002	58.5 ± 0.2	103.9 ± 0.6	102 ± 1	0.792 ± 0.007
10	RA 106/2	4.66 ± 0.03	0.841 ± 0.001	0.566 ± 0.003	61.0 ± 0.3	95.2 ± 0.8	93 ± 2	0.765 ± 0.005
11	S 19/1	6.40 ± 0.10	0.88 ± 0.01	0.56 ± 0.01	319 ± 68	92 ± 3	–	0.85 ± 0.03
12	RA 107	5.70 ± 0.03	0.884 ± 0.001	0.517 ± 0.002	733 ± 3	81.6 ± 0.4	–	0.854 ± 0.004
13	S 20/1	12.60 ± 0.30	0.88 ± 0.01	0.475 ± 0.007	820 ± 290	71 ± 2	–	0.85 ± 0.03
14	RA 102	7.42 ± 0.05	0.915 ± 0.001	0.472 ± 0.002	1814 ± 6	70.9 ± 0.3	–	0.896 ± 0.004
15	S 11/2	5.70 ± 0.10	0.87 ± 0.01	0.469 ± 0.008	375 ± 100	70 ± 2	–	0.84 ± 0.03
16	S 19/2	10.20 ± 0.20	0.897 ± 0.007	0.44 ± 0.01	730 ± 325	65 ± 2	–	0.88 ± 0.03
17	S 20/6	4.60 ± 0.20	0.91 ± 0.01	0.35 ± 0.02	21 ± 3	46 ± 3	–	0.90 ± 0.06
18	RA 1	12.50 ± 0.30	0.8396 ± 0.0074	0.3149 ± 0.0042	84 ± 9	41.6 ± 0.7	–	0.82 ± 0.02
19	RA 109	8.29 ± 0.04	0.863 ± 0.001	0.0934 ± 0.0004	118.4 ± 0.6	10.79 ± 0.05	10.7 ± 0.1	0.859 ± 0.004
20	RA 108	9.39 ± 0.05	0.836 ± 0.001	0.0928 ± 0.0003	61.5 ± 0.2	10.72 ± 0.04	10.53 ± 0.08	0.831 ± 0.003
21	RA 32	11.18 ± 0.04	0.8187 ± 0.0008	0.0885 ± 0.0007	43.6 ± 0.4	10.19 ± 0.09	10.0 ± 0.2	0.813 ± 0.007
22	RA 31	10.06 ± 0.04	0.814 ± 0.001	0.0787 ± 0.0006	84.4 ± 0.7	9.02 ± 0.08	8.9 ± 0.2	0.809 ± 0.007
23	RA 19	5.63 ± 0.02	0.819 ± 0.001	0.0321 ± 0.0003	190 ± 2	3.56 ± 0.04	3.55 ± 0.04	0.817 ± 0.009
	Veľký Dóm chamber							
24	VD 15	7 ± 1	0.90 ± 0.03	1.04 ± 0.04	600 ± 180	>350 (<1.2 Ma)	–	–
25	VD Zeb. (surface layer)	0.98 ± 0.07	1.070 ± 0.05	0.90 ± 0.04	238 ± 117	237^{+30}_{-25}	–	1.14 ± 0.13
26	VD Pol 1	11.56 ± 0.02	1.018 ± 0.001	0.4538 ± 0.0009	897 ± 2	65.63 ± 0.20	–	1.022 ± 0.003
27	VD Pol 2	6.79 ± 0.01	0.967 ± 0.001	0.2612 ± 0.0007	10232 ± 29	32.98 ± 0.10	–	0.964 ± 0.003
28	VD-13/1 base	11.2 ± 0.3	0.85 ± 0.01	0.113 ± 0.002	98 ± 15	13.0 ± 0.2	–	0.84 ± 0.02
29	VD-14/1 base	0.88 ± 0.04	1.09 ± 0.04	0.090 ± 0.007	14 ± 4	10.2 ± 0.9	9 ± 2	1.1 ± 0.2
30	BH 1B	1.50 ± 0.06	1.054 ± 0.037	0.0569 ± 0.0060	184 ± 280	6.4 ± 0.7	–	1.06 ± 0.12

Fig. 3. Outcrop of the cave sidebar and location of main logs (upper picture), with the allostratigraphic nine sedimentary units distinguished and mapped in the outcrop (lower diagram); the tenth unit is the gravel lag of the incised modern underground river. Note the location (red points) and dates of speleothem samples; sample numbers as in Table 1.

Sedimentological description

Unit 1 – This oldest exposed unit, dated to >349 ka by its earliest speleothem cap (log II, Fig. 3), occurs in the sidebar downstream part (see outcrop segment with logs I and II in Fig. 3). Its maximum thickness exposed above the present-day river level is ~50 cm (log II), but a hand-drill probing indicates that its base reaches a few more decimetres below the river floor and that its true maximum thickness may be around 80 cm. In the downstream direction, this unit abuts against and covers a bedrock knoll protruding as a low-relief ridge (azimuth ~275°) from the cave eastern wall. Similar is the trend of Unit 1, which extends as a mound obliquely (azimuth ~290°) from the cave wall into the outcrop (cf. Fig. 3). The deposits of this unit are clast-supported, sand-filled pebble gravel with an admixture of cobbles (local D_{max} = 11 cm to 25 cm; Fig. 4) and with a 'rolling' clast

fabric *a*(t)*b*(i) (Fig. 5A) indicating local bedload transport towards the WNW. The top of Unit 1 is erosional with an irregular relief, draped by speleothems ranging in age from 349 ka to 305 ka (Fig. 3).

Unit 2 – This second unit is sandy and occurs as a speleothem-draped erosional remnant, 15 cm thick, at the site of log II – with the flowstone drape extending to log I (Fig. 3). The sediment is fine-grained sand, light brownish grey in colour, with a few thin intervening layers of flowstone cementation (Figs 4 and 5B). The basal flowstone layer, dated to 349 ka, has bedding attitude of 175/10° and the upper flowstone layer of 200/30°, indicating an upward-steepening upstream sand accretion with episodes of emergence. The earliest flowstone layer draping this unit's erosional escarpment (Fig. 5B) is dated to 236 ka (Fig. 3, log II).
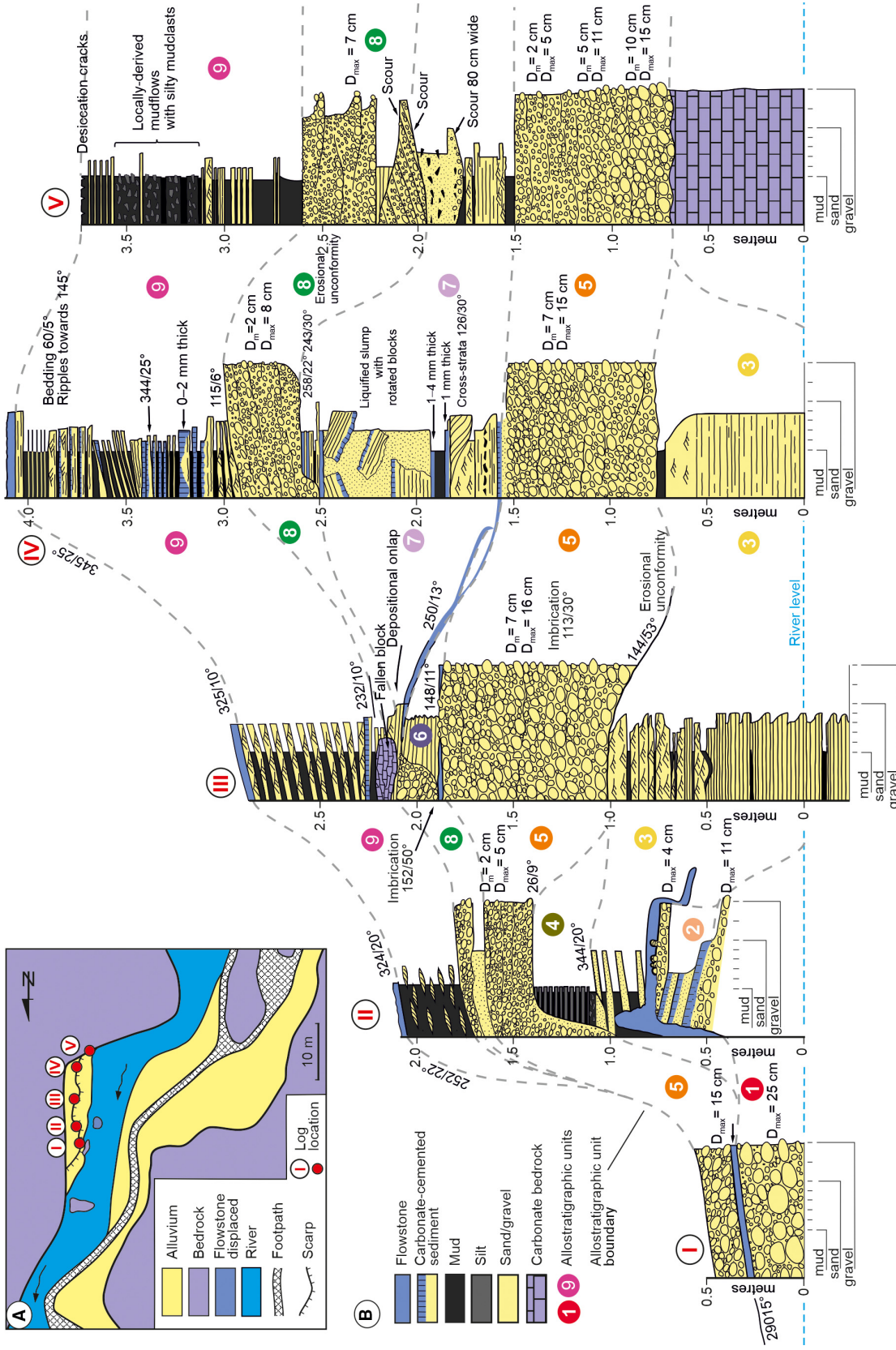
Fig. 4. (A) Location map of the sidebar preserved at the right-hand (eastern) bank of underground river-bend niche in the Prízemie cave segment, with approximate position of outcrop logs. (B) Detailed sedimentological logs of the sidebar escarpment outcrop; the coloured numbers of allostratigraphic units are as in Fig. 3; D_m and D_{max} are the local mean and maximum clast sizes, respectively; the other numerical values are measurements of the dip azimuth and dip angle of bedding surfaces and clast imbrication.
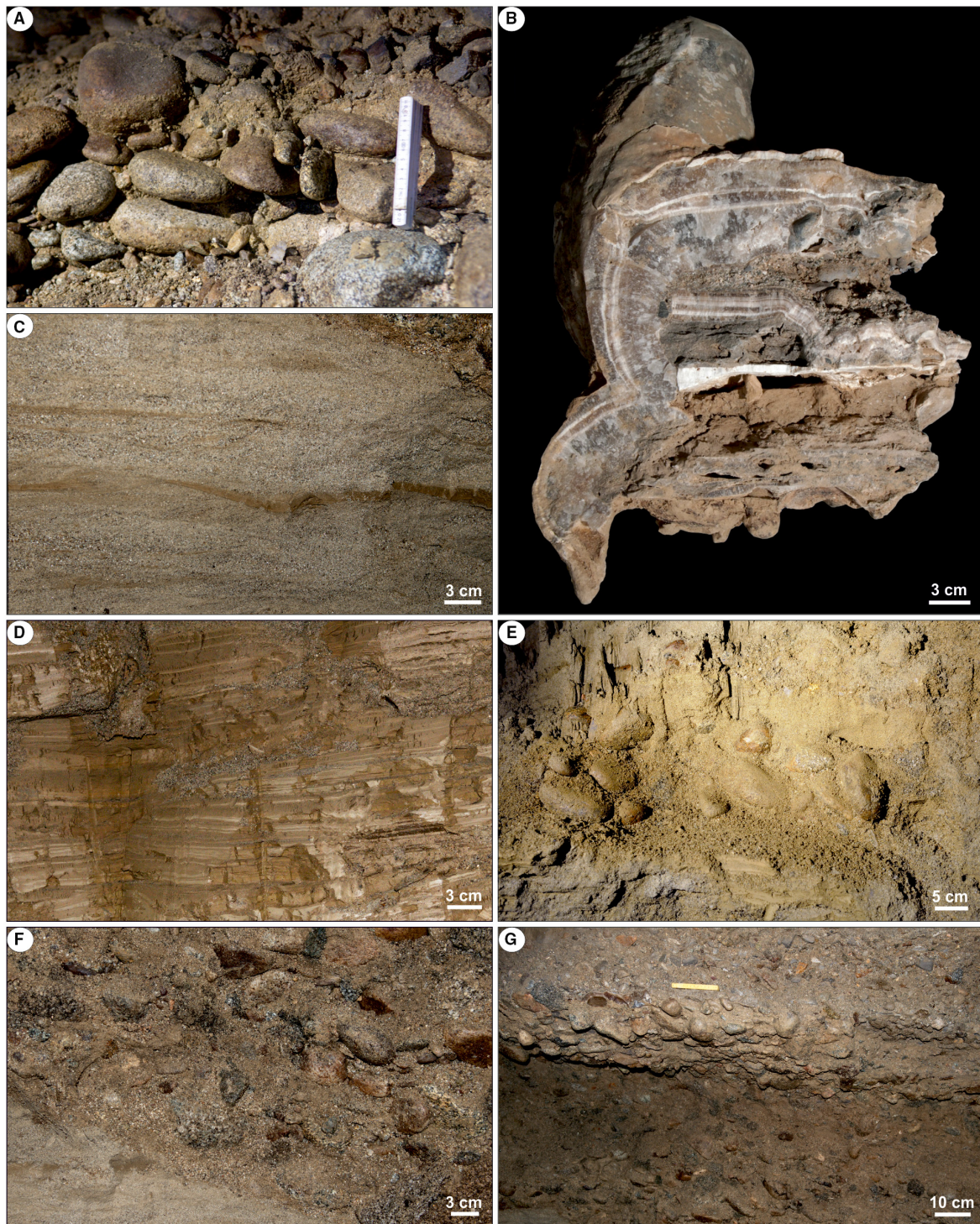
Fig. 5. Close-up facies details of allostratigraphic units 1 to 6 (Fig. 3). (A) Imbricate gravel of Unit 1 in log I (Fig. 4); the measuring stick (scale) is 10 cm. (B) The top part of Unit 2, with flowstone horizons, overlain by thin gravel lag of Unit 3, escarped by erosion (to the left), draped by speleothem and overlain by the younger hetero-lithic sand-mud facies of Unit 3; sample extracted from outcrop in log II (Fig. 4). (C) Detail of Unit 3 in log III (Fig. 4), with parallel-stratified coarse sand overlain by mud-draped, ripple cross-laminated sand layers. (D) Detail of the sand-mud heterolithic Unit 4 in log II (Fig. 4). (E) Detail of the gravelly Unit 5 underlain by cross-laminated sandy unit 4 in log II (Fig. 4). (F) Detail of the gravelly Unit 5 overlying unconformably the sandy Unit 3 in log III (Fig. 4). (G) The gravelly Unit 5 overlain directly by Unit 8 in log III (Fig. 4). Outcrop logs as in Figs 3 and 4.

Fig. 6. Succession of allostratigraphic units in the vicinity of log III (Fig. 4), showing flowstone-separated units 5 and 6 overlain with a low-relief erosional escarpment by units 8 and 9. Note the limestone blocks (Fb) fallen from the cave roof at the base of Unit 9. Hammer (35 cm) for scale. Allostratigraphic units as in Fig. 3. Flowstone layers are highlighted in light blue. Speleothem samples with dates (red dots) are numbered as in Table 1.

Unit 3 – This next unit extends laterally almost throughout the outcrop section, from between logs I/II to between logs IV/V (Fig. 3), and reaches a thickness of up to 1.1 m above the present-day river level in log III. The depth of its true base in logs III and IV is unknown, where also the unit top is markedly erosional, overlain directly by Unit 5 (Fig. 3). Unit 3 in log II is less than 40 cm thick and overlies an erosional terrace that is a local remnant of the two older units (Fig. 3). The terrace is covered with a lag of pebble gravel (D_{max} = 4 cm) draped by speleothems dated to 182.4 ka and overlain by a package of alternating thin sand and mud layers inclined towards 344°, with a steepening-upward dip angle of up to 20° (Fig. 4). In log IV, the exposed upper part of Unit 3 is 75 cm thick and consists of planar parallel-stratified coarse-grained sand fining upward into ripple cross-laminated fine/medium sand (Fig. 5C) and overlain by mud (Fig. 4). In the intermediate log III, the parallel-stratified sand varies from coarse-grained to medium-grained with sporadic mud interlayers, and the cross-laminated uppermost part of the unit contains several such thin muddy interlayers (Fig. 4). The basal speleothem, at the top of Unit 2 (Fig. 3, log II), indicates a lower time limit of 182.4 ka, but the exact upper time limit for the deposition of Unit 3 is unknown.

Unit 4 – This unit is preserved between logs II and III as an erosional remnant only 0.30 m thick (Fig. 3), but is very meaningful, as it overlies Unit 3 and yet is the finest-grained, composed of thinly interlayered dark brownish-grey clayey mud and lighter-shade muddy silt (Figs 4 and 5D). The bedding is flat and nearly horizontal, commencing with a thin (5 cm) basal layer of chaotic, massive mud bearing scattered silty mudclasts. This unit clearly post-dates Unit 3 and pre-dates Unit 5 (Fig. 3), but lacks bounding speleothems in the outcrop.

Unit 5 – This next unit has a distinctly erosional base, with a relief exceeding 1 m, and extends laterally throughout the outcrop (Fig. 3). It consists of a light brownish-grey, clast-supported and sand-filled coarse pebble gravel (Fig. 5E and G; local D_{max} = 5 to 16 cm, Fig. 4) with crude plane-parallel stratification. Imbricate *a*(t)*b*(i) clast fabric (140/45° in log II and 113/30° in log III, Fig. 4) indicates local bedload transport towards the north-west. The erosional base of this unit is deepest-incised in log I, where it reaches down to ~0.3 m above the present-day river level and directly overlies the flowstone-draped Unit 1 (Figs 3 and 4). The base is least incised in log II, about 1.3 m above the modern river level, and reaches down to less than 1 m above the river level in logs III to V (Figs 3 and 4). This unit clearly post-dates Unit 4, and the oldest speleothems at its top are 102 ka in age.

Unit 6 – This unit is preserved only in log III, as a flowstone-draped discontinuous sand wedge less than 0.3 m thick and pinching out towards log IV (Fig. 3), with bedding attitude 250/13° (Fig. 4). The sand is medium-grained to coarse-grained, with planar parallel stratification, and overlies the flowstone-draped top of Unit 5 dated to between 102 ka and 93 ka
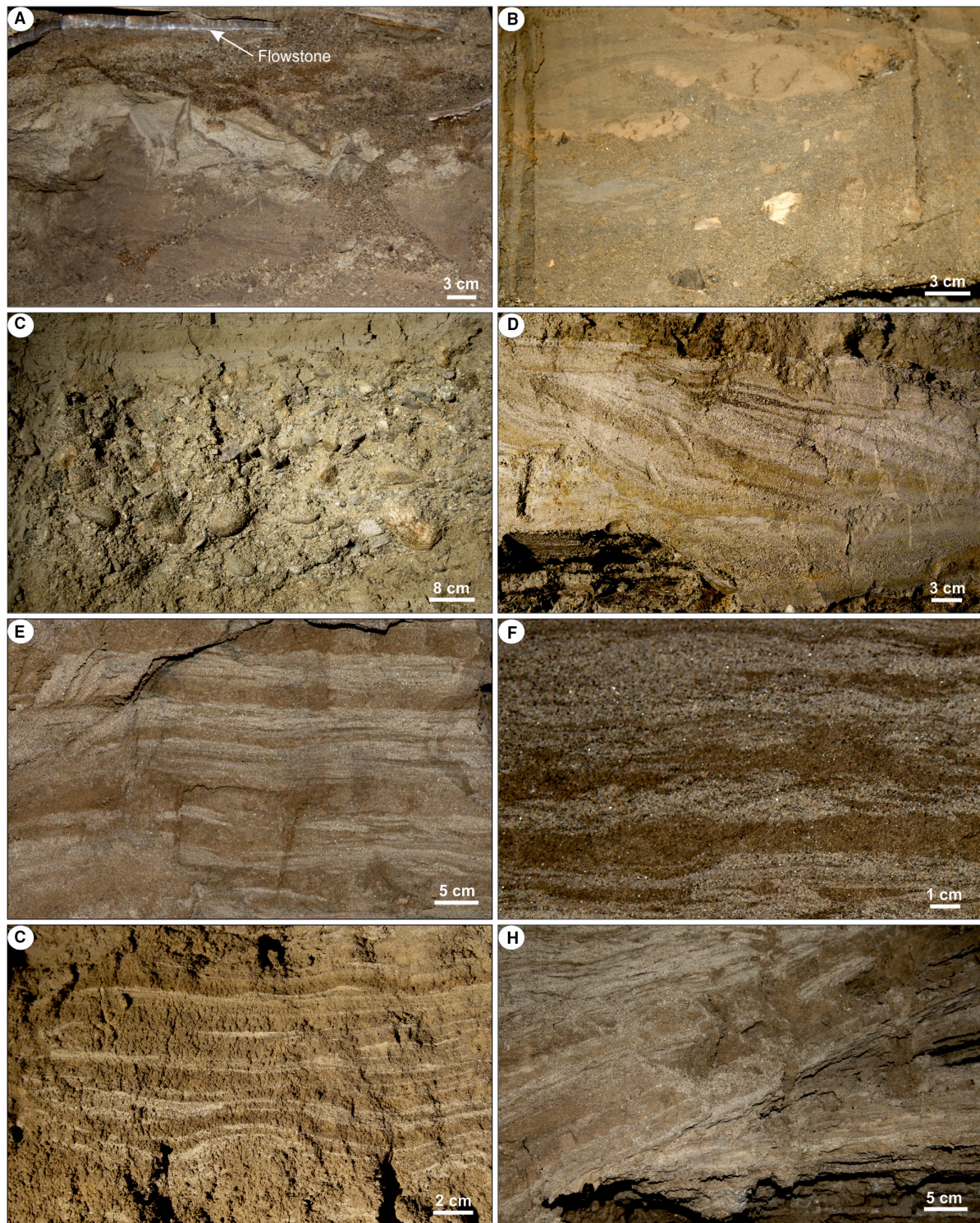
Fig. 7. Close-up facies details of allostratigraphic units 7 to 9 (Fig. 3). (A) The upper part of slump deposit separated by flowstone layer from the overlying stratified sand in Unit 7 (log IV, Fig. 4). (B) The lower part of slump deposit in Unit 7, with disrupted sand lenses and flowstone debris (same locality). (C) The gravelly Unit 8 overlain by sand-dominated heterolithic facies of Unit 9 (log IV, Fig. 4). (D) The heterolithic Unit 9 between logs IV and V. (E). Unit 9 in log III. (F) Ripple cross-lamination in the sandy layers in Unit 9 between logs IV and V. (G) Slight soft-sediment deformation in Unit 9 near the top of log V. (H) Unit 9 foreset between logs III and IV. Outcrop logs as in Figs 3 and 4.

(Figs 3 and 6). The flowstone cover of Unit 6 in log III has an age range of 81.6 to 70 ka (Figs 3 and 6). These dates would then define the time bracket for the deposition of Unit 6.

Unit 7 – This unit extends laterally from log III, where it shows depositional onlap on the flowstone-draped Unit 6, to the upstream end of the outcrop – where it overlies the flowstone-covered Unit 5 and reaches a thickness of 1.2 m in log IV (Figs 3 and 4). The component sedimentary facies show great variation. The lower part of Unit 7 consists of fine-grained to coarse-grained sand with ripple cross-lamination and plane-parallel stratification, including mud interlayers (up to 5 cm thick) and thin flowstone drapes, and with trough-shaped isolated shallow scours filled with a solitary cross-strata set (log IV) or non-stratified pebbly coarse sand (log V, Fig. 4). The upper part of this unit consists of massive (non-stratified) sand, which is fine-grained and bears rotated blocks of partly cemented and flowstone-draped stratified sand in log IV (Fig. 7A and B), and is medium-grained and rich in mudclasts in log V (Fig. 4). The topmost part of Unit 7, preserved as an erosional relic only in log IV (Fig. 4), is a heterolithic package of thinly interlayered fine-grained sand and mud with a few intervening horizons of flowstone cementation. The onlapping base of Unit 7 between logs IV and III is slightly diachronous, from 70.9 to 70 ka, whereas a flowstone drape near its top in log IV has an age of 41.6 ka (Fig. 3). The time span of Unit 7 is then from 70 ka to at least 41.6 ka.

Unit 8 – This gravelly unit has a basal erosional relief of around 1 m and extends laterally from log II to log V (Fig. 3), with a maximum thickness of 0.7 m in log V and a virtual downstream pinch-out towards log I. The gravel has a sand-filled clast-supported texture (Figs 6 and 7C), varies from granule to pebble grade (D_{mean} = 2 cm, D_{max} = 8 cm) and shows clast imbrication fabric a(t)b(i) trending 152/50° (Fig. 4), indicating gravel transport towards the north-west. According to the bounding speleothem ages, the minimum time bracket for the deposition of Unit 8 would be between 41.6 and 10.7 ka (Fig. 3).

Unit 9 – This unit is mud-rich and heterolithic, composed of thinly interlayered mud and cross-laminated fine-grained sand (Figs 6 and 7E to G). It extends laterally from log V to log II, reaching a maximum thickness of 1.2 m in log IV (Fig. 3) and marking the highest water stand of the river. The finest-grained deposits of

Unit 9, in log V (Fig. 4), include massive (non-laminated) mud layers with abundant silty mud-clasts. The base of this unit shows fallen cave-roof limestone blocks (log III, Figs 4 and 6). The heterolithic deposits of Unit 9 form a sigmoidal large-scale bed set of 'microdelta' type (*sensu* Jopling, 1965), with the bottom-set attitude of 325/6°, foreset attitude of 344/25° and topset attitude of 60/5° (Fig. 7D and H). The topset contains some ripple cross-sets directed obliquely upstream, towards 145°. The top surface of Unit 9 shows desiccation cracks in log V and is covered by a flowstone layer with stalagmites in logs II to IV (Fig. 4), dated to 3.56 ka (Fig. 3). The deposits also contain a few thin flowstone interlayers and carbonate-cemented horizons with dates of 10.7 to 8.9 ka. According to the speleothem dates (Fig. 3), the time bracket for the deposition of Unit 9 would be between 10.7 ka and 3.56 ka, although the top surface of this unit continues to accumulate flowstone today.

Unit 10 – This youngest unit is a gravelly pavement of the incised, modern subterranean Demänovka River (Figs 3 and 4A). It consists mainly of coarse pebbles and small cobbles, sub-rounded to well-rounded, and has a clast-supported, sand-filled texture. Hand-drill probing indicates gravel thickness of around 0.3 m, with an underlying sand probably representing Unit 3 (cf. Fig. 3). This unit clearly post-dates the latest major incision of the subterranean Demänovka River.

Morphodynamic interpretation
The morphodynamic development of sedimentation in the cave conduit is summarized schematically as an interpretive cartoon in Fig. 8. Unit 1 is older than 354 ka and interpreted as the downstream part of an early gravelly sidebar mound (Fig. 8A) formed in the flow separation zone of the cave conduit bend (cf. Fig. 4A). This bar abutted on a transverse bedrock knoll and buried it (Fig. 3). The overlying Unit 2 has an age range between 354 ka and 236 ka and is interpreted as a sandy scroll-bar accreted obliquely in an upstream direction to the cross-cave protrusion relief of the earlier gravelly sidebar (Fig. 8B). The river water level at this stage was lower and fluctuated, as indicated by the flowstone drapes (Fig. 4B) recording temporal emergence.

Unit 3 recorded an episode of cave-wide erosional reactivation of the river, leaving a gravel lag on the terrace made of units 1/2 in log II and
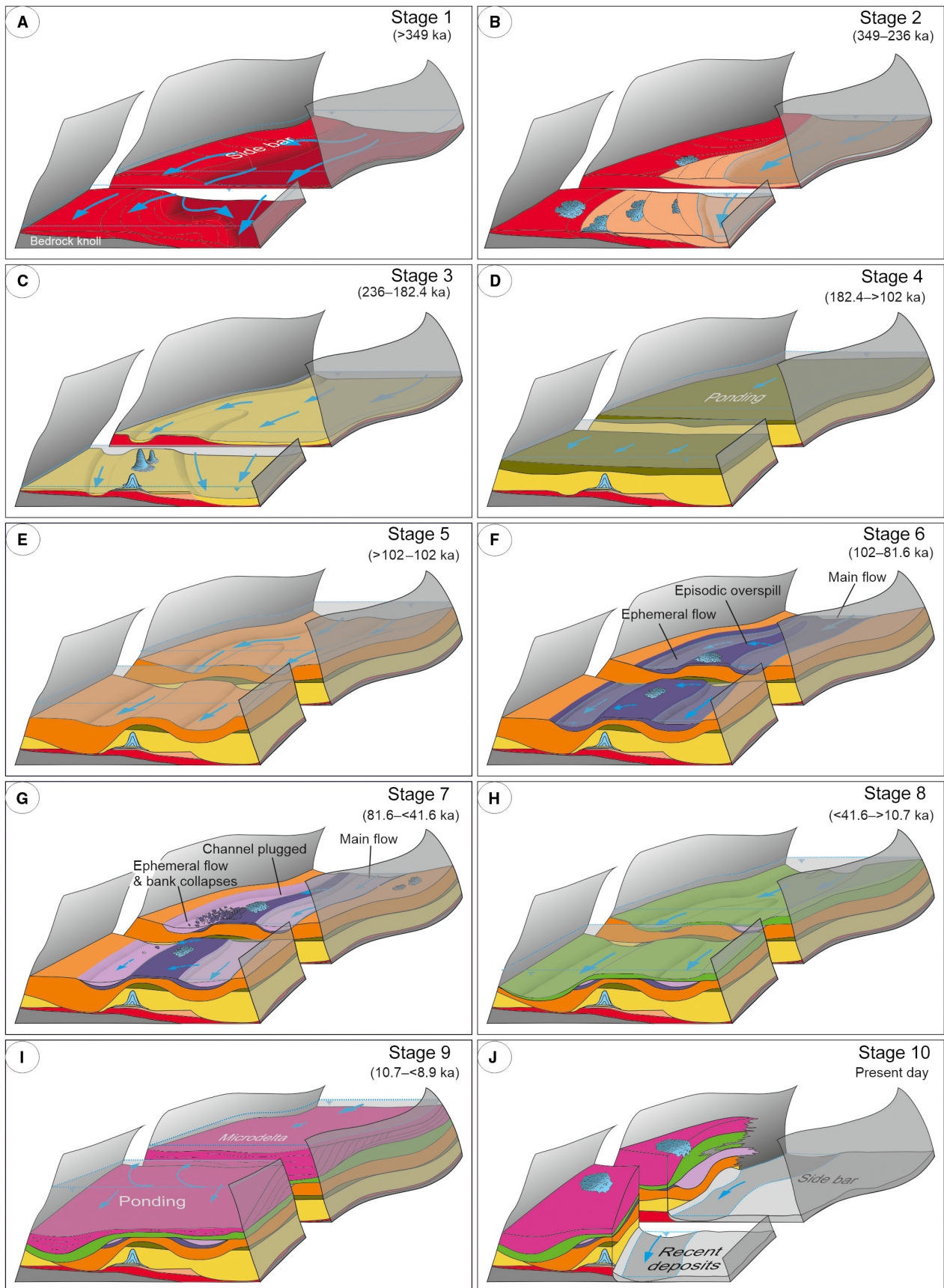
Fig. 8. Schematic cartoon summary of the interpreted sedimentation morphodynamics and hydrological conditions in the Prízemie segment of the DCS. (A) Stage 1 (>349 ka): a gravelly sidebar forms in the flow separation zone at the cave bend (cf. Fig. 4A). (B) Stage 2 (349 to 236 ka): a mid-channel sand-gravel bar forms at the river bend, spilling out sand towards the channel right-hand bank. (C) Stage 3 (236 to 182.4 ka): an erosional sand-bed channel shifts to its right-hand cave wall while maintaining also its flow route between the two earlier-formed bars, with flowstone patches and stalagmites formed initially outside these channel branches. (D) Stage 4 (182.4 to >102 ka): cave-wide aggradation of fluvial sand culminates in a flow-ponding episode of mud deposition, attributed to downstream cave-roof collapse (Fig. 9). (E) Stage 5 (>102 to 102 ka): the river break-through occurs and its flow is reactivated, scouring the substrate as two channel branches while spreading gravel over the whole cave width. (F) Stage 6 (102 to 81.6 ka): the river level falls and flow decreases, with speleothem flowstone patches forming on channel banks (G) Stage 7 (81.6 to <41.6 ka): the river channel banks are emerged and collapsing, with the near-wall channel branch increasingly ephemeral, plugged by a slowly advancing mid-channel sand bar. (H) Stage 8 (<41.6 to >10.7 ka): the gravel-bed river is reactivated, with substrate scouring and cave-wide gravel deposition. (I) Stage 9 (10.7 to <8.9 ka): a new episode of flow ponding (high-stage slack water conditions), with progradation of a channel-filling silt-mud microdelta (*sensu* Jopling, 1965), attributed to the flow blocking by another downstream cave-roof collapse (cf. Fig. 9). (J) Present-day stage of incised river with its channel-floor gravel lag and left-bank sidebar as the youngest depositional unit. Diagrams not to scale; the cave width there is about 25 m and the thickness of preserved terraced deposits is ~4 m. Time ranges based on speleothem U-series isotopic dating.

---

forming a short-lived chute channel near the right-side (eastern) cave wall, while incising its thalweg towards the cave axis and left-side wall (Figs 3 and 8C). The flow then subsided and became confined to the thalweg zone, whereby the abandoned chute and erosional intrachannel

terrace emerged and were covered by speleothems including prominent stalagmites (log II, Fig. 3). The time bracket of this development was 236 to 182.4 ka. The water level subsequently rose and a cave-wide river aggradation occurred, with a heterolithic channel-bank levée
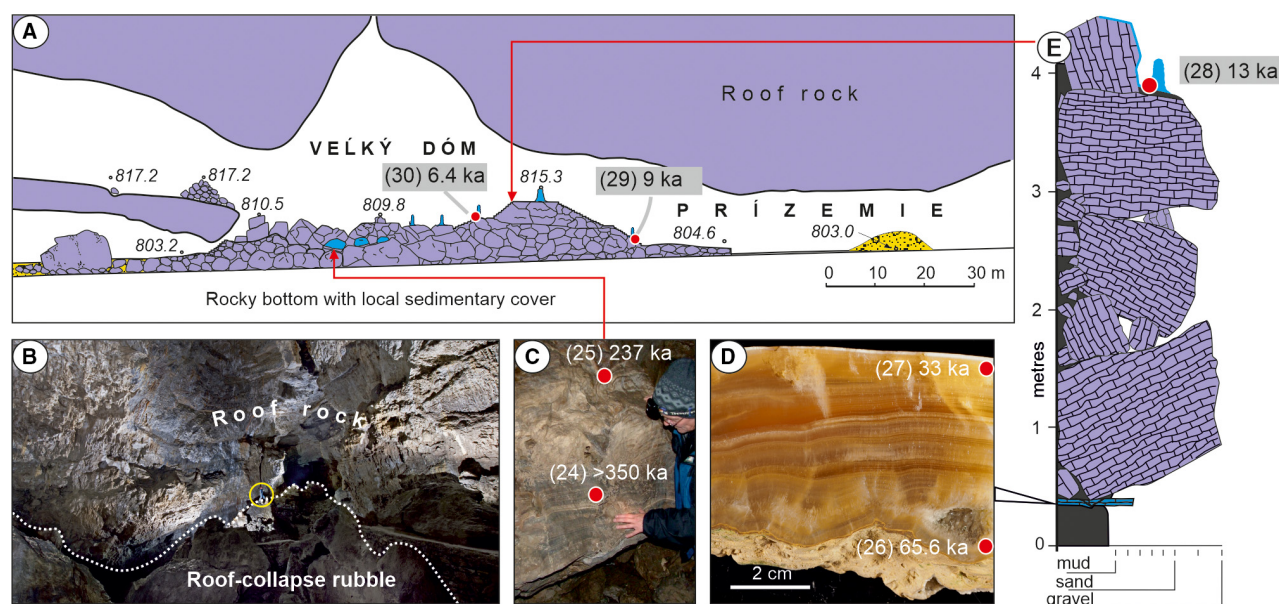
Fig. 9. (A) Longitudinal cross-section through the studied segment of cave conduit (Fig. 2), showing the sidebar relic in Prízemie in relation to the pile of cave-roof collapse breccia in downstream Veľký Dóm chamber. The black-point values indicate local altitude (in metres) and the grey-shaded red-point values are U-series dates of breccia-top speleothems. Speleothems and speleothem blocks are marked with pale blue. (B) Upstream view of the Veľký Dóm chamber, with a standing person (encircled, *ca* 1.8 m tall) for scale. Photograph courtesy of P. Stanik. (C) Displaced and rotated flowstone block in the lower part of the breccia with U-series dates (sample numbers as in Table 1). (D) Close-up view of the flowstone layer beneath the youngest part of breccia pile and its U-series date range. (E) Simplified vertical log of the youngest part of breccia pile in Veľký Dóm chamber with a rock-block speleothem date.

built obliquely towards the cave right-hand wall and burying the speleothems (Fig. 4B). This marked sidebar depositional aggradation, between 182.4 and ~160 ka, heralded the subsequent stage of pronounced water-level rise and flow ponding recorded by the muddy Unit 4 (Figs 3, 4 and 8D).

Unit 4 recorded pulsating high-stage slackwater conditions, attributed to the abrupt retardation and virtual blocking of the river flow by a barrier of cave roof-collapse breccia in the downstream Veľký Dóm segment of the cave conduit (Fig. 9A). The chaotic basal muddy layer in Unit 4 (Fig. 4) is a mudflow deposit derived from the rapidly submerged earlier channel-bank levée. The ponding stage is poorly constrained by speleothems, but its time bracket is estimated at between ~160 and ~140 ka. The Veľký Dóm chamber (Fig. 9A and B) was apparently prone to multiple roof failures. The collapse breccia blocks there bear displaced speleothems post-dating 237 ka, with the younger recognizable collapses post-dating 33 ka and draped by flowstones younger than 13 ka (Fig. 9C to E).

Unit 5 recorded an abrupt erosional reactivation of a gravel-bed river, attributed to the water eventually breaking through the downstream breccia barrier in the Veľký Dóm transit chamber (Fig. 9A). The local transport directions of the unit's bedload gravel indicate main flow to the north-west. This implies a river flow guided again by the cave conduit bend and conforming to the pre-existing erosional terrace made of Units 1 to 4, which also made the river channel split into two erosive branches: a deeper one at the right-hand (eastern) side of the conduit and a shallower one diverted obliquely towards its left-hand side (Figs 4 and 8E). The time bracket for the deposition of gravelly Unit 5 is estimated as ~140 ka until ~120 ka.

Unit 6, preserved only in log III (Fig. 4), was apparently deposited in its main volume in the cave near-wall sector around log I, but was subsequently removed by later erosion. The stratified relic of this unit in log III, dipping towards the WSW and pinching out towards log IV (Fig. 3), is a sand wedge spilled over into the abandoned 'hanging' channel of Unit 5 (Fig. 8F) – which episodically emerged, as indicated by flowstone drapes (Fig. 4). As an interpretive inference, the main, non-preserved part of Unit 6 in the outcrop sector of logs I and II was probably gravelly to coarse sandy, reaching a cumulative height of up to 1.5 m above the

reference level of present-day river to cause eventually the overspill of sand. The net time bracket for stage 6 (Fig. 8F) would be ~120 until 70 ka, with the time bracket for clastic sedimentation between 93 ka (youngest flowstone at the top of Unit 5) and 81.6 ka (oldest flowstone at the top of Unit 6; Figs 3 and 6).

Unit 7 is a heterolithic facies assemblage indicating ephemeral flow with episodes of slackwater conditions, emergence and flowstone deposition (Fig. 8G). The main flow of an aggrading river channel at that time (70 ka until 41.6 ka) was apparently near the cave western wall, where the main sedimentary volume of Unit 7 was deposited but is unpreserved. The outcrop sector between logs III and V shows a perched terrace with the pre-existing 'hanging' channel – plugged with sediment at the upstream bend, periodically emerged (speleothems) and recording only episodic sand overspill flow of the river thalweg. The deposition of massive sand with mudclasts (log V, Fig. 4) and with flowstone-draped rotated sand blocks (log IV, Fig. 4) indicates liquefied slumps derived from the perched channel's emerged margins. The main sediment body of Unit 7, as well as that of Unit 6, in the outcrop sector of logs I and II was removed by the erosional emplacement of Unit 8 (Figs 3 and 4).

Unit 8 represents a gravelly palaeochannel that first strayed away from the eastern wall towards the cave axis (logs IV–V sector of the outcrop, Fig. 3), and then cut down back towards this wall (logs I–III sector), removing the pre-existing deposits of units 5 to 7 and leaving only a thin gravel lag in logs II and III. The channel apparently reached an incision bypass stage and accumulated only sparse gravel pavement, with clast imbrication indicating bedload transport towards the NNW (Fig. 4). The capping speleothem above Unit 8 is dated to 10.7 ka (Fig. 3), but the high-relief base of this unit is hiding a considerable erosional gap, whereby the latest preserved speleothem (41.6 ka) of the relic Unit 7 below cannot be regarded as a true lower-boundary date for Unit 8 itself. The high water discharge of stage 8 (Fig. 8H) commenced probably not before ~20 ka.

Unit 9 represents a mud-rich 'microdelta' that prograded downstream from the cave conduit bend. Its deposition alternated between frictional tranquil flow (Wright, 1977) and slackwater conditions, as it gradually filled in the near-wall scour relief created at the previous stage

(Fig. 8I). The formation of this unit indicates flow ponding (high-stage slackwater conditions), attributed to yet another episode of cave-roof collapse and flow damming in the downstream Veľký Dóm segment of the cave conduit (Fig. 9). The evidence of fallen roof-rock blocks at the base of Unit 9 in the Prízemie segment of the cave (Fig. 6, and log III in Fig. 4) supports this interpretation. Internal speleothem drapes (log IV, Fig. 4) indicate water-level fluctuations, with temporal topset emergence and a related emplacement of delta slope-derived mudflows (log V, Fig. 4). The reverse-flow ripple cross-lamination in the microdelta topset (log IV, Fig. 4) indicates a reversing water circulation in the river-flow entrapment and separation zone of the cave bend (Fig. 8I). Unit 9 clearly post-dates Unit 8 (Fig. 3) and pre-dates the subsequent deep river incision and emplacement of gravelly Unit 10. The youngest speleothem inter-layer ~20 cm beneath the top of the resulting erosional terrace (log IV) is dated to 8.9 (±0.2) ka, which means that the river level still oscillated around 2.5 m above its present level. Almost immediately followed the river deep incision of stage 10 (Fig. 8J), as indicated by the stalagmite growth ~2.5 m above the present river level about 60 m downstream from the studied section and post-dating the ponding episode (date sample 29 in Fig. 9A).

Unit 10, much like the earlier Unit 8, recorded another dramatic incision of the subterranean river, this time towards the cave left-hand (western) wall and resulting in the present-day morphology of the Prízemie passage (Fig. 8J). Sidebar undercutting caused local displacement of large flowstone fragments onto the river floor (Fig. 3). This major erosional event is attributed to the river's new episode of breaking through its downstream roof-collapse breccia barrier (Fig. 9). The gravel lag of Unit 10 indicates a temporal end of river local incision and a switch to depositional mode, although the hydraulic profile of the subterranean river will inevitably evolve further by morphological adjustment.

DISCUSSION

The river profile

Underground bedrock fluvial systems are generally the locus of the most rapid change in the drainage basin and – in regional scale – they control the spatial propagation of base-level change (Tinkler & Wohl, 1998; Ford & Willliams, 2007). The longitudinal profile of the active underground conduit in the DCS, between the river southern inlet and its northern karst-spring outlet (Fig. 2), is notably more concave upward and deeper incised than the corresponding profile of the surface stem of the river (Droppa, 1966, 1972; Hochmuth, 1993, 1997). The DCS inflow zone shows an upstream-rising hydraulic gradient of the underground subhorizontal epiphreatic or looped phreatic conduits, as compared to the surface river, with several ponors and vadose drawdown passages (Bella, 1993). The intersection point of the underground and the subaerial river profiles is in the downstream Veľký Dóm chamber (Fig. 2), where the steady-state earlier incision of the underground river was perturbed by a roof-collapse rubble barrage (Fig. 9A). The barrage broke down the river profile, established a local temporary base level and disturbed underground incision by knickpoint upstream migration (Fig. 2). The underground river stem with a perennial flow has been able to regulate its profile more efficiently than the parallel surface river stem that is periodically dry. Downstream of the river resurgence to the surface, its profile has regulated to the valley base level by another knickpoint (Fig. 2). The karst spring is at an altitude of 789 m, near the mouth of the right-hand side valley, and has a cascade morphology of knickpoint incision by 3 to 4 m. The resurging river there joins the subaerial river stem and its profile. In addition to the two main knickpoints (Fig. 2), both the underground and the resurging surface river profiles show an array of secondary knickpoints in the form of recessing bedrock steps less than 0.5 m in relief (Bella, 2019).

The roof collapse in the Veľký Dóm chamber was a multi-episode phenomenon, although the limited access to the rubble barrage interior (Fig. 9A and B) allows only the youngest episode to be dated based on speleothems. This youngest pile of rubble, up to 4 m thick, overlies an impact-crashed flowstone layer dated to 33 ka and is covered by a flowstone with stalagmites dated to 13 ka (Fig. 9D and E). The fallen blocks bear rotated cave-roof flowstone drapes with a wide range of ages (Fig. 9C). The two distinct episodes of flow ponding in the upstream Prízemie passage – commencing around 180 ka and 10 ka, respectively (Fig. 8) – were apparently a result of the main successive roof collapses and flow damming stages in the Veľký Dóm chamber (cf. Fig. 9A).
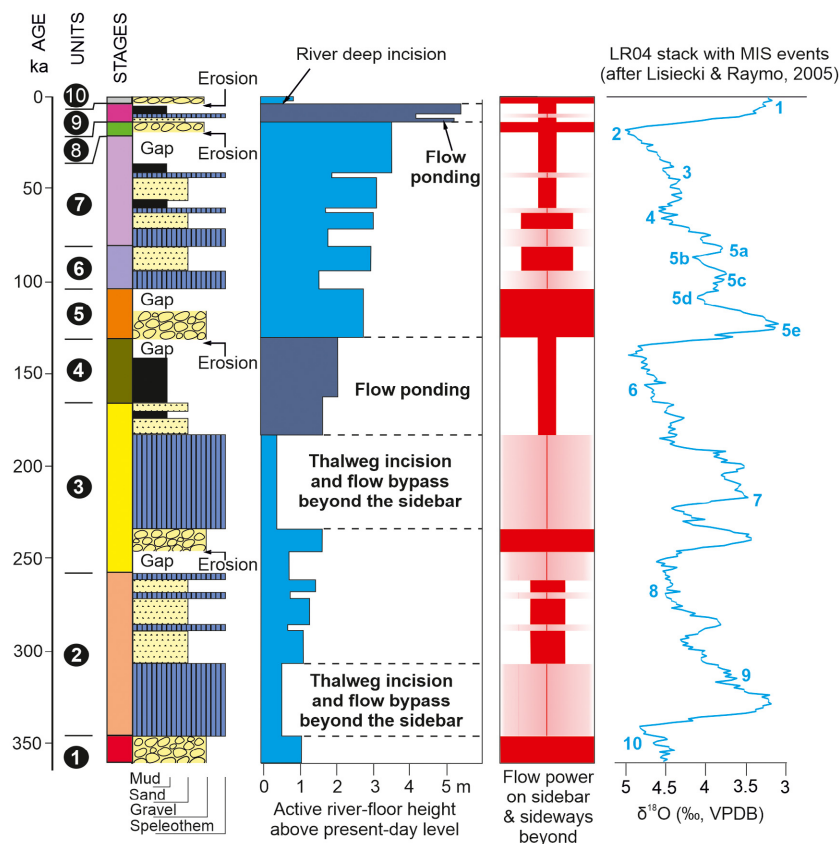
Fig. 10. Hydrological interpretation of the cave conduit's post-350 ka history in relation to the North Atlantic climate record (LR04 stack with MIS redrawn from Lisiecki & Raymo, 2005). The estimation of active river-floor height relative to its present-day level is based on the maximum height of particular allostratigraphic units in the sidebar outcrop. The estimation of flow power is qualitative, comparing flow over the sidebar (plot in red) with the inferred contemporaneous flow of river thalweg incised beyond the bar area (plot in pink).

The flow-ponding sedimentary record (units 4 and 9, Fig. 4) indicates fluctuations of the contemporaneous river water level and energy between a sand-carrying weak tranquil flow and mud-depositing slackwater conditions. The barrage at each episode of roof collapse must have been initially an openwork feature, gradually patched with the river bedload gravel and sand, and eventually filled in with mud (Fig. 9E). However, the barrier permeability varied due to the local washout of its interstitial sand and mud by filtrating water flow. As the river fluctuating water level behind the barrier was critically rising in the Veľký Dóm chamber, a sufficient breakthrough of flow eventually occurred to terminate the ponding episode.

The water percolating through the cave roof today is oversaturated with calcium and forming speleothems, but the river water is undersaturated (Motyka *et al.*, 2005) and hence dissolving both carbonate debris and the cave limestone bedrock. Similar hydrochemistry was likely the case during the warmer periods of the Pleistocene and may have contributed to the river breaking through the cave barrage. One can predict that once the barrage is eliminated by washout, corrasion, abrasion and dissolution, the

local intersection point (Fig. 2) will vanish and the whole underground to subaerial river profile will eventually be regulated towards a joint equilibrium and the valley downstream general base level.

The cave roof collapses were most probably triggered by regional earthquakes, as is common in karst caves (e.g. Kagan *et al.*, 2005; Becker *et al.*, 2006, 2012; Frumkin, 2009; Martelli *et al.*, 2012; Domenica & Pizzi, 2017; Camelbeeck *et al.*, 2018). The Carpathians with its Tatra Mountains range are a young Alpine mountain belt subject to neotectonic activity driven by post-orogenic crustal relaxation. Regional seismo-tectonic activity since the Pliocene is well-documented (e.g. Gradziński *et al.*, 2014; Szczygieł, 2015), including the record of recent earthquakes (Kováč *et al.*, 2002; Guterch, 2009; Wiejacz & Dębski, 2009; Hók *et al.*, 2016).

Speleothem record

The compound-bar stratigraphic succession (Fig. 10) shows seven recognizable generations of speleothems. They record relatively warm and humid land-surface conditions, with a vegetation cover and carbonate bedrock dissolution

by percolating water and with the re-precipitation of calcium carbonate as speleothems in the cave (Fairchild & Baker, 2012). These generations are broadly correlative with the warming phases of north-west European climate (see the plot of marine isotope stages, MIS, in Fig. 10; Lisiecki & Raymo, 2005), although there are also some notable discrepancies – probably due to specific local or regional conditions. For example, the oldest, first speleothem generation commenced its precipitation well before the global warming shown by deep-marine record, while the second generation apparently corresponds to the cool period MIS 8 (Fig. 10).

However, the Scandinavian glaciation at that time reached no farther south than central Poland and has virtually no record in southern Germany (Eismann, 2002). Contemporaneous glaciations in the Tatra Mountains have been suggested (Marks *et al.*, 2016, fig. 5), but the local caves show formation of speleothems at that time. If mountain glaciers did exist in the Carpathians, they must have been short-lived and of limited extent (Szczygieł *et al.*, 2019; Błaszczyk *et al.*, 2020). Speleothems formed contemporaneously in the Alps (Spötl & Mangini, 2007), where recognizable significant cooling occurred at the closure of MIS 8 (*ca* 240 to 230 ka), indicating short-lived glaciers.

A well-developed generation of three successive speleothems, with thick flowstone layers and stalagmites up to 70 cm high, formed between 236 ka and 182.4 ka, during the warm period of MIS 7 (Fig. 10). Coeval growth of numerous speleothems occurred in Central European caves in the Alps (Spötl & Mangini, 2007; Spötl *et al.*, 2008) and the Tatra Mountains (Kicińska *et al.*, 2017; Szczygieł *et al.*, 2019).

The younger part of the studied succession contains four generations of flowstone layers, dated to 102 to 93 ka, 81 to 70 ka, ~41.6 ka and the Holocene, which correspond roughly to the MIS warming phases 5c, 5a, 3 and 1 (Fig. 10). Coeval precipitation of speleothems occurred in other parts of the DCS (Hercman *et al.*, 1997, 2006; Hercman, 2000; Podgórska, 2019), as well as in the caves of the Tatra Mountains (Głazek, 1984; Hercman *et al.*, 2008) and the Alps (e.g. Moseley *et al.*, 2014). These four youngest generations of speleothems in the present case formed on the emerged bar surface, which means that the river apparent low water stages were due to its thalweg lateral incision away from the bar (Fig. 8).

Somewhat puzzling may seem the lack of speleothems correlative with MIS 5e (Fig. 10), which – according to the European pollen record – was the warmest and most humid episode of MIS 5 (Helmens, 2014), corresponding to the Eemian interglacial. The reason was probably the cave bar submergence by an erosive high-level flow of undersaturated river water (Fig. 8). Speleothems of this age are known from other parts of the DCS (Hercman *et al.*, 2006).

Cave hydrology and regional climatic implications

Based on the speleothems and vertical facies changes, ten stages of sedimentation are recognizable in the Prízemie passage (Fig. 10). Their sedimentary record is allostratigraphic units 1 to 10 (cf. Figs 3 and 8), which include episodes of emergence as well as stratigraphic gaps due to erosion or sediment bypass. The units give a proxy record of the cave-conduit hydrological conditions (Fig. 10). The active river-floor level relative to its present-day position, as reached through the successive stages, is estimated from the maximum measured height of particular sedimentary unit and the height of speleothems (emergence levels) in the sidebar outcrop. These estimates approximate the river minimum water level. The qualitative estimation of relative flow-power changes is based on sedimentary facies.

The vertical organization of facies in the cave sidebar shows a characteristic motif of erosively emplaced gravel lag covered directly by a flowstone layer (Fig. 10), which indicates tunnel-wide erosional rejuvenation of powerful flow followed by the river thalweg sideways incision, with the water level fall, sidebar emergence and cave-roof water percolation. The formation of contemporaneous speleothems implies wet land-surface conditions. The flowstone cover, recording sidebar emergence, is overlain by sandy facies alternating with flowstone drapes, which indicates low-power flow and river-floor net aggradation with a fluctuating water level. Aggradation in karstic rivers is generally linked to cool periods (Harmand *et al.*, 2017). These episodes correlate with the periods MIS 10, 8, 6 and 2 (Fig. 10). In the regional context of the Low Tatra Mountains, this cave-fill facies motif may indicate climatic warming to cooling phases. In addition came the meaningful random episodes of flow ponding due to cave-roof collapses, probably recording major regional earthquakes (Fig. 10), with the initial infilling of

rubble barrage by fluvial sediments and a subsequent river breakthrough.

Notably, there is no evidence of permafrost formation in the cave tunnel. The deposits show no cryoturbation, such as described from freezing caves (e.g. Luetscher, 2013; Obu *et al.*, 2018), and there are no cryogenic cave carbonates that might indicate temporal formation of ice in the tunnel. The extent of permafrost in the Western Carpathians during the last glaciation is uncertain, and some other parts of the multilevel DCS may have been locally and ephemerally frozen (Orvošová *et al.*, 2014). However, the pollen studies of intermountain peat bogs in the Western Carpathians document the presence of forests during the last glaciation (Jankovská *et al.*, 2002; Jankovská & Pokorný, 2008). The allogenic DCS was located at the mountain glacier front that constantly provided water to the karst system, during the ice-front advance, stillstand and retreat. The concentrated water flux probably transferred heat to the cave by advection (Domínguez-Villar, 2012), as exemplified by the Castleguard Cave in the Canadian Rocky Mountains (see Yonge *et al.*, 2018, fig. 15.32). The latter cave is located below the Columbia Icefield, yet the temperature in the vast part of its interior is above 0°C.

The gravel Unit 1 (Fig. 10) is older than 349 ka, but speleothem cover ages (Fig. 3) indicate that its top was reworked with minor gravel accretion around 349 ka (MIS 9). The bulk of this unit is apparently a cave-side relic record of the early Pleistocene (pre-MIS 10) melting of mountain glaciers. Little is known about these early mountain glaciations in Europe, but it is generally accepted that the Scandinavian Ice Sheet had its greatest southward extent in Central Europe during MIS 16 (676 to 621 ka) and MIS 12 (478 to 424 ka) (see review by Böse *et al.*, 2012). In Poland, the Scandinavian Ice Sheet is considered to have reached the Carpathian foothills during the glaciations Sanian 1 and Sanian 2, correlated with MIS 16 and MIS 12, respectively (Marks, 2011; Lindner & Marks, 2015; Marks *et al.*, 2016). Marks (2011) and Marks *et al.* (2016) suggested coeval glaciations in the Tatra Mountains, although direct surface evidence of these mountain glaciations in Europe is lacking. Their only proxy relic record may then be the underground fluvial deposits.

Similar is apparently the significance of the gravelly Unit 3 and Unit 5, recording a retreat of mountain glaciers at the warming phases of MIS 7 and MIS 5e, respectively (Fig. 10). The erosional gravel of Unit 3 correlates with the melting of small Alpine glaciers around 230 ka (cf. Spötl & Mangini, 2007). The age frame of Unit 5 is imprecise, but this stage of underground flow rejuvenation correlates with the final peak of penultimate deglaciation in the Central European mountains (cf. Böse *et al.*, 2012), dated from the Alpine speleothems to between ~137 ka (Häuselmann *et al.*, 2015) and ~134 ka (Spötl *et al.*, 2002; Moseley *et al.*, 2015). This timeframe corresponds well with the erosional emplacement of Unit 5 (Fig. 10). The surface record of mid-Pleistocene mountain glaciations in the Alps and Carpathians is poor, erased by younger erosion (Louček *et al.*, 1960; Droppa, 1972; Schlüchter, 2008). The Scandinavian Ice Sheet supposedly made significant advances in the area of Germany and The Netherlands (Böse *et al.*, 2012), and may have even sneaked into the Czech territory through the Moravian Gate in southern Poland (Marks *et al.*, 2019). On the other hand, coeval cave speleothems in the Tatra Mountains (Hercman *et al.*, 2008; Kicińska *et al.*, 2017) and Outer Carpathians (Gradziński *et al.*, 2012) indicate lack of permafrost and a relatively mild regional climate, perhaps weakly seasonal.

The gravelly Unit 8 correlates with the onset of MIS 1 (Fig. 10). The erosional base of this unit reached destructively flowstone layers dated to 41.6 ka, and its sandy cover contains thin flowstone layers dated to 10.7 ka (Fig. 3). Landforms and surface deposits of the preceding glaciation are common in the Low Tatra Mountains (Louček *et al.*, 1960), but remain there undated. The [10]Be exposure age of glacial maximum moraines in the High Tatra Mountains is between ~20 ka (Engel *et al.*, 2015; Makos *et al.*, 2018) and 18 ka (Engel *et al.*, 2017). The oldest Late Pleistocene postglacial speleothems in the DCS have ages between 15 ka and 13.5 ka (Hercman *et al.*, 2020). The deglaciation phase MIS 1 in the Low Tatra Mountains would then occur between ~20 ka and 15 ka, which matches the timeframe of Late Pleistocene glacier demise in the Alps (Ivy-Ochs *et al.*, 2004; Wirsig *et al.*, 2016; Fabbri *et al.*, 2018).

The erosional incision of gravelly Unit 10 (Fig. 10) recorded the post-glacial onset of Holocene hydrography, combined with the river break through the downstream roof-collapse barrage. This stage of sedimentation in the cave conduit marked the development of the modern river profile, as discussed in a previous section.
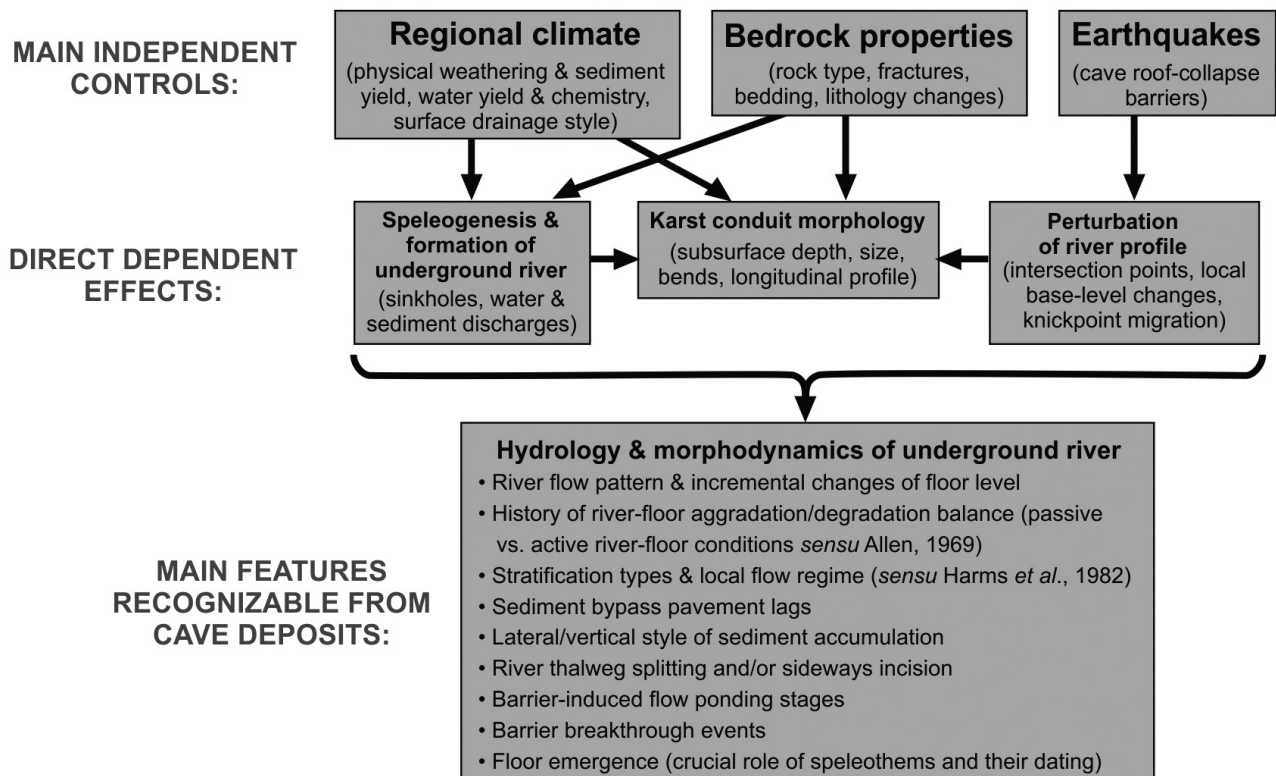
Fig. 11. Principal controls on an underground fluvial system, with a tentative list of the river hydrological and morphodynamic features recognizable from its cave deposits.

Rivers underground

The main independent controls on cave fluvial systems (Fig. 11, top; cf. Ford & Willliams, 2007) are similar to those acting on surface bedrock rivers (Tinkler & Wohl, 1998; Jansen, 2006; Whipple *et al.*, 2013), where barriers can form by gorge-side rockslides. Bedrock river channels are generally considered to be fundamentally different from alluvial river channels, with the latter being shaped principally by water flow and sediment transport processes and the former principally by lithological and structural bedrock controls (Richards, 1982; Baker & Pickup, 1987; Ashley *et al.*, 1988). The range of geological, environmental and geomorphic factors controlling surface alluvial rivers is thus different and wider (Richards, 1982; Schumm, 1985; Tooth *et al.*, 2004; Bridge., 2009; Nicholas *et al.*, 2018). Alluvial rivers have their channels cut in floodplain sediments, potentially mobile, and have the capability to migrate laterally or shift position by abrupt avulsion. The morphology of bedrock river channels, in broad terms, is a direct compromise negotiated between the fluvial forces applied and bedrock resistance offered (Tinkler &

Wohl, 1998). The underground rivers may locally behave in an alluvial style in wider passages and large chambers (Ghinassi *et al.*, 2009), but not in the cave-linking narrower conduits that predominate the subsurface extent of karst fluvial systems.

Bedrock rivers, even at quite low stages, typically show greater flow velocities and shear stresses than alluvial rivers (Ashley *et al.*, 1988; Tinkler & Wohl, 1998). In contrast to alluvial river channels, the width of bedrock conduit is nearly invariant and its vertical accommodation space for a rising water level is practically unlimited. The morphodynamic response to hydraulic change at a falling water stage is limited to the appearance of a narrow thalweg zone, its braided-style splitting or localized incision. The flow in bedrock systems is unsteady and non-uniform and is commonly referred to as transcritical (Tinkler & Wohl, 1998), because it involves sections that are hydraulically critical, supercritical or subcritical. The transcritical regime is important, as it generates flow perturbations and causes flow superelevation at bends, which in alluvial channels dissipates by overbank spill-out.

The most specific and crucial dependent control on underground bedrock rivers is the speleogenesis (Ford & Willliams, 2007), with its sinkhole pattern of water and sediment supply and its direct impact on cave conduit morphology (Fig. 11). An allogenic karst system with a hydraulic gradient receives water and sediment mainly from an upstream non-karstic drainage terrain. The sinking river can switch abruptly to a deeper cave conduit through vadose drawdown passages (Ford & Ewers, 1978; Ford, 2000), whereby its underground longitudinal profile evolves independently of the parallel surface river-stem profile (Fig. 2). The underground and surface river stems are joining one another beyond the karst spring zone, where a knickpoint forms and a common new downstream river profile is hydraulically negotiated. It is also speleogensis, combined with random independent perturbations (roof-collapse barrages, bedrock lithological changes and possibly active cross-faults), that determines the underground river profile and its evolution (Fig. 11). Underground channel bends are not simple ingrown natural meanders (Brakenridge, 1985), but features imposed by speleogenesis and bedrock characteristics.

Underground bedrock rivers are an extreme end-member case of the continuum of alluvial and bedrock channels (Brakenridge, 1985; Ashley *et al.*, 1988). Their deposits provide a unique sedimentological opportunity to study the behaviour of a fluvial system arrested in a bedrock confinement, where the river evolution and hydrological history are a response to a limited number of specific controlling factors and are recorded within a single bedrock conduit. As the present case study demonstrates, even the local relic cave deposits provide a whole range of crucial geological information (Fig. 11, lower part) – with direct implications for the cave system hydrological history and regional climatic conditions.

Particularly interesting will be conceptual considerations as to how the least action principle (LAP), manifested by maximum flow efficiency (Nanson & Huang, 2017), plays its governing geomorphic role in a bedrock-confined underground fluvial system. Furthermore, the existing stream power models for surface alluvial rivers rely heavily on the substitution of water discharge for drainage area (Anthony & Granger, 2007). The style of channel incision and knickpoint migration in sinkhole-fed underground fluvial conduits, controlled by speleogenesis, may differ significantly from that in alluvial rivers and hence calls for a closer analytical consideration. The definition of karst-spring catchment area and boundaries has long been a major problem in the karst hydrology and hydrogeology, similarly begging for a new careful consideration (Bonacci & Andrić, 2015).

CONCLUSIONS

The present study demonstrates that a detailed sedimentological analysis of the relic cave-fill fluvial deposits can be an important contribution to speleological research and to an understanding of the hydrological history of karstic-cave river conduits. The study shows that the underground Quaternary fluvial deposits can provide an important proxy record of the regional history of glaciations and climatic changes. From a regional perspective, the study sheds a new light on the history of mountain glaciations and deglaciations in the Demänová Valley of the Low Tatra Mountains, which was a subject of long-time literature speculations and controversies, and which may have regional climatic implications for the whole Central European Carpathians.

This is the first speleological study documenting a direct time link of the cave-fill gravelly facies motif with the climate warming phases, surface catchment deglaciation and rejuvenation of fluvial drainage. Another significant facies motif is that of aggradational sandy deposits indicating lower flow regime and water level fluctuations during cold climate phases, as well as the random slackwater facies motif of flow ponding, related to major cave-roof collapses and indicating regional earthquakes.

The study encourages sedimentological research of underground fluvial systems, which have thus far been little explored and for which the dating of speleothems, facies analysis and knowledge of bedrock rivers prove to be invaluable for both local hydrological and regional climatic reconstructions.

ACKNOWLEDGEMENTS

reviews with editorial comments from Nick Eyles and Peir Pufahl helped to improve the manuscript.

DATA AVAILABILITY STATEMENT

The data that support the findings of this study are available from the corresponding author upon reasonable request.

REFERENCES

Anthony, D.M. and **Granger, D.E.** (2007) An empirical stream power formulation for knickpoint retreat in Appalachian Plateau fluviokarst. *J. Hydrol.*, **343**, 117–126.

Ashley, G.M., **Renwick, W.H.** and **Haag, G.H.** (1988) Channel form and processes in bedrock and alluvial reaches of the Raritan River, New Jersey. *Geology*, **16**, 436–439.

Assaad, F.A. and **Jordan, H.** (1994) Karst terranes and environmental aspects. *Environ. Geol.*, **23**, 228–237.

Auler, A.S., **Smart, P.L.**, **Wang, X.**, **Piló, L.B.**, **Edwards, R.L.** and **Cheng, H.** (2009) Cyclic sedimentation in Brazilian caves: mechanisms and palaeoenvironmental significance. *Geomorphology*, **106**, 142–153.

Backwell, L., **d'Errico, F.** and **Wadley, L.** (2008) Middle stone age bone tools from the Howiesons Poort layers, Sibudu Cave, South Africa. *J. Archaeol. Sci.*, **35**, 1566–1580.

Baker, V.R. and **Pickup, G.** (1987) Flood geomorphology of the Katherine Gorge, northern territory, Australia. *Geol. Soc. Am. Bull.*, **98**, 635–646.

Barton, H.A. and **Northup, D.E.** (2007) Geomicrobiology in cave environments: past, current and future perspectives. *J. Cave Karst Stud.*, **69**, 163–178.

Becker, A., **Davenport, C.A.**, **Eichenberger, U.**, **Gilli, E.**, **Jeannin, P.-Y.** and **Lacave, C.** (2006) Speleoseismology: a critical perspective. *J. Seismol.*, **10**, 371–388.

Becker, A., **Häuselmann, P.**, **Eikenberg, J.** and **Gilli, E.** (2012) Active tectonics and earthquake destructions in caves of northern and central Switzerland. *Int. J. Speleol.*, **41**, 35–49.

Bella, P. (1993) Remarks on the genesis of the Demänova Cave System. *Slov. Kras*, **31**, 43–53. [In Slovak, with English abstract.].

Bella, P. (2019) Morphological and developmental differences within the lower parts of Demänovská jaskyňa slobody Cave along the Demänovka underground stream. *Aragonit*, **24/2**, 20–26. [In Slovak, with English abstract.].

Bella, P., **Haviarová, D.**, **Kováč, L.**, **Lalkovič, M.**, **Sabol, M.**, **Soják, M.**, **Struhár, V.**, **Višňovská, Z.** and **Zelinka, J.** (2014a). Caves of the Demänová Valley. Štátna Ochrana Prírody SR, Správa Slovenských Jaskýň, Liptovský Mikuláš, 200 pp. [In Slovak, with English summary.].

Bella, P., **Hercman, H.**, **Gradziński, M.**, **Pruner, P.**, **Kadlec, J.**, **Bosák, P.**, **Głazek, J.**, **Gąsiorowski, M.**, **Nowicki, T.** and **Šlechta, S.** (2014b) Rekonštrukcia hlavných vývojovývh fáz jaskynného systému. In: *Caves of the Demänová Valley* (Eds Bella, P., Haviarová, D., Kováč, Ľ., Lalkovič, M., Sabol, M., Soják, M., Struhár, V., Višňovská, Z. and Zelinka, J.), pp. 47–53. Štátna Ochrana Prírody SR, Správa Slovenských Jaskýň, Liptovský Mikuláš. [In Slovak, with English summary.].

Bird, M.I., **Boobyer, E.M.**, **Bryant, C.**, **Lewis, H.A.**, **Paz, V.** and **Stephens, W.E.** (2007) A long record of environmental change from bat guano deposits in Makangit Cave, Palawan, Philippines. *R. Soc. Edinburgh Trans. Earth Environ. Sci.*, **98**, 59–69.

Błaszczyk, M., **Hercman, H.**, **Pawlak, J.** and **Szczygieł, J.** (2020) Palaeoclimate reconstruction in the Tatra Mountains (Western Carpathians, Poland) during MIS 9–7 inferred from multiproxy speleothem records. *Quatern. Res.*, doi.org/10.1017/qua.2020.69.

Bögli, A. (1980) *Karst Hydrology and Physical Speleology*. Springer-Verlag, Berlin, 286 pp.

Böse, M., **Lüthgens, C.**, **Lee, J.R.** and **Rose, J.** (2012) Quaternary glaciations of northern Europe. *Quatern. Sci. Rev.*, **44**, 1–25.

Bonacci, O. and **Andrić, I.** (2015) Karst spring catchment: an example from Dinaric karst. *Environ. Earth Sci.*, **74**, 6211–6223.

Bosch, R.F. and **White, W.B.** (2004) Lithofacies and transport of clastic sediments in karstic aquifers. In: *Studies of Cave Sediments: Physical and Chemical Records of Paleoclimate* (Eds Mylroie, J.E. and Sasowskyr, I.D.), pp. 1–22. Kluwer, New York.

Brakenridge, G.R. (1985) Rate estimates for lateral bedrock erosion based on radiocarbon ages, Duck River, Tennessee. *Geology*, **13**, 111–114.

Bridge, J.S. (2009) *Rivers and Floodplains: Forms, Processes, and Sedimentary Record*. John Wiley & Sons, New York, 504 pp.

Camelbeeck, T., **Quinif, Y.**, **Verheyden, S.**, **Vanneste, K.** and **Knuts, E.** (2018) Earthquakes as collapse precursors at the Han-sur-Lesse Cave in the Belgian Ardennes. *Geomorphology*, **308**, 13–24.

Cheng, H., **Lawrence Edwards, R.**, **Shen, C.C.**, **Polyak, V.J.**, **Asmerom, Y.**, **Woodhead, J.**, **Hellstrom, J.**, **Wang, Y.**, **Kong, X.**, **Spötl, C.**, **Wang, X.** and **Calvin Alexander, E.** (2013) Improvements in ^{230}Th dating, ^{230}Th and ^{234}U half-life values, and U-Th isotopic measurements by multi-collector inductively coupled plasma mass spectrometry. *Earth Planet. Sci. Lett.*, **371–372**, 82–91.

Collinson, J.D., **Mountney, N.P.** and **Thompson, D.B.** (2006) *Sedimentary Structures* (3rd edn). Terra Publishing, Harpenden, 292 pp.

Cruz Jr, F.W., **Burns, S.J.**, **Karmann, I.**, **Sharp, W.D.**, **Vulle, M.**, **Cardaso, A.O.**, **Ferrari, J.A.**, **Dias, P.L.S.** and **Vlana Jr, O.** (2005) Insolation-driven changes in atmospheric circulation over the past 116,000 years in subtropical Brazil. *Nature*, **434**, 63–65.

Di Domenica, A. and **Pizzi, A.** (2017) Defining a mid-Holocene earthquake through speleoseismological and independent data: implications for the outer Central Apennines (Italy) seismotectonic framework. *Solid Earth*, **8**, 161–176.

Domínguez-Villar, D. (2012) Heat flux. In: *Speleothem Science: From Process to Past Environments* (Eds Fairchild, I. and Baker, A.), pp. 137–145. Wiley-Blackwell, Chichester.

Droppa, A. (1957) *Die Höhlen Demänovské Jaskyne*. Vydavatelstvo Slovenskej Akademie Vied, Bratislava, 289 pp. [In Slovak with German summary.].

Droppa, A. (1966) The correlation of some horizontal caves with river terraces. *Stud. Speleol.*, **1**, 186–192.

Droppa, A. (1972) Die geomorphologischen Verhältniosse im Demänovská-Tal. *Slov. Kras*, **10**, 9–46. [In Slovak, with English abstract.].

Eismann, L. (2002) Quaternary geology of eastern Germany (Saxony, Saxon-Anhalt, South Brandenburg, Thuringia), type area of the Elsterian and Saalian stages in Europe. *Quatern. Sci. Rev.*, **21**, 1275–1346.

Engel, Z., **Mentlík, P.**, **Braucher, R.**, **Křížeka, M.**, **Pluháčková, M.** and **Team, A.** (2015) Geomorphological evidence and [10]Be exposure ages for the Last Glacial Maximum and deglaciation of the Velká and Malá Studená dolina valleys in the High Tatra Mountains, central Europe. *Quatern. Sci. Rev.*, **124**, 106–123.

Engel, Z., **Mentlík, P.**, **Braucher, R.**, **Křížeka, M.**, **Pluháčková, M.** and **Team, A.** (2017) [10]Be exposure age chronology of the last glaciation of the Roháčská Valley in the Western Tatra Mountains, central Europe. *Geomorphology*, **293**, 130–142.

Fabbri, S.C., **Buechi, M.W.**, **Horstmeyer, H.**, **Hilbe, M.**, **Hübscher, C.**, **Schmelzbach, C.**, **Weiss, B.** and **Anselmetti, F.S.** (2018) A subaquatic moraine complex in overdeepened Lake Thun (Switzerland) unravelling the deglaciation history of the Aare Glacier. *Quatern. Sci. Rev.*, **187**, 62–79.

Fairchild, I.J. and **Baker, A.** (2012) *Speleothem Science: From Process to Past Environments.* Wiley-Blackwell, Chichester, 432 pp.

Ford, D.C. (2000) Speleogenesis under unconfined settings. In: *Speleogenesis. Evolution of Karst Aquifers* (Eds Klimchouk, A.B., Ford, D.C., Palmer, A.N. and Dreybrodt, W.), pp. 319–324. National Speleological Society, Huntsville.

Ford, D.C. and **Ewers, R.O.** (1978) The development of limestone cave systems in the dimensions of length and depth. *Can. J. Earth Sci.*, **15**, 1783–1798.

Ford, D. and **Willliams, P.** (2007) *Karst Hydrogeology and Geomorphology.* John Wiley & Sons, Chichester, 562 pp.

Frumkin, A. (2009) Formation and dating of a salt pillar in Mount Sedom diaper, Israel. *Geol. Soc. Am. Bull.*, **121**, 286–293.

Gaál, Ľ. (2016) Lithology of carbonate rocks of Demänová Cave System. *Slov. Kras*, **54**, 109–129. [In Slovak, with English abstract.].

Gaál, Ľ. and **Michalík, J.** (2017) Middle Triassic limestones in the Okno Cave (Demänovská dolina Valley, Low Tatras): lithology and facies types. *Slov. Kras*, **55**, 145–154. [In Slovak, with English abstract.].

Ghinassi, M., **Colonese, A.C.**, **Giuseppe, Z.D.**, **Govoni, L.**, **Vetro, D.L.**, **Malavasi, G.**, **Martini, F.**, **Ricciardi, S.** and **Sala, B.** (2009) The Late Pleistocene clastic deposits in the Romito Cave, southern Italy: a proxy record of environmental changes and human presence. *J. Quatern. Sci.*, **24**, 383–398.

Głazek, J. (1984) First isotope datings of speleothems from Tatra caves and their bearing on Pleistocene stratigraphy of the Tatra Mts. *Przegl. Geol.*, **32**, 39–43. [In Polish, with English summary.].

Goldberg, P. and **Sherwood, S.C.** (2006) Deciphering human prehistory through the geoarcheological study of cave sediments. *Evol. Anthropol.*, **15**, 20–36.

Gradziński, M., **Duliński, M.**, **Hercman, H.**, **Górny, A.** and **Przybyszowski, S.** (2012) Peculiar calcite speleothems filling fissures in calcareous sandstones and their palaeohydrological and palaeoclimatic significance: an example from the Polish Carpathians. *Geol. Quart.*, **56**, 711–732.

Gradziński, M., **Wróblewski, W.**, **Duliński, M.** and **Hercman, H.** (2014) Earthquake-affected development of a travertine ridge. *Sedimentology*, **61**, 238–263.

Guterch, B. (2009) Seismicity in Poland in the light of historical record. *Przegl. Geol.*, **57**, 513–520. [In Polish, with English abstract.].

Haeuselmann, P., **Granger, D.E.**, **Jeannin, P.Y.** and **Lauritzen, S.E.** (2007) Abrupt glacial valley incision at 0.8 Ma dated from cave deposits in Switzerland. *Geology*, **35**, 143–146.

Häuselmann, A.D., **Fleitmann, D.**, **Cheng, H.**, **Tabersky, D.**, **Günther, D.** and **Edwards, R.K.** (2015) Timing and nature of the penultimate deglaciation in a high alpine stalagmite from Switzerland. *Quatern. Sci. Rev.*, **126**, 264–275.

Harmand, D., **Adamson, K.**, **Rixhon, G.**, **Jaillet, S.**, **Losson, B.**, **Devos, A.**, **Hez, G.**, **Calvet, M.** and **Audra, P.** (2017) Relationships between fluvial evolution and karstification related to climatic, tectonic and eustatic forcing in temperate regions. *Quatern. Sci. Rev.*, **166**, 38–56.

Harmon, R.S. and **Wicks, C.M.** (Eds) (2006) Perspectives on karst geomorphology, hydrology, and geochemistry: a tribute volume to Derek C. Ford and William B. White. *Geol. Soc. Am. Spec. Pap.*, **404**, 366.

Harms, J.C., **Southard, J.B.**, **Spearing, D.R.** and **Walker, R.G.** (1975) Depositional Environments as Interpreted from Primary Sedimentary Structures and Stratification Sequences. SEPM Short Course No. 2 Lecture Notes, 161 pp.

Harms, J.C., **Southard, J.B.** and **Walker, R.G.** (1982) Structures and Sequences in Clastic Rocks. SEPM Short Course No. 9 Lecture Notes, 250 pp.

Hellstrom, J. (2003) Rapid and accurate U/Th dating using parallel ion-counting multi-collector ICP-MS. *J. Anal. At. Spectrom.*, **18**, 1346–1351.

Helmens, K.F. (2014) The Last Interglacial-Glacial cycle (MIS 5–2) reexamined based on long proxy records from central and northern Europe. *Quatern. Sci. Rev.*, **86**, 115–143.

Hercman, H. (2000) Reconstruction of palaeoclimatic changes in central Europe between 10 and 200 thousand years BP, based on analysis of growth frequency of speleothems. *Studia Quatern.*, **17**, 35–70.

Hercman, H., **Bella, P.**, **Głazek, J.**, **Gradziński, M.**, **Lauritzen, S.-E.** and **Løvlie, R.** (1997) Uranium series dating of speleothems from Demanova ice cave: a step to age estimation of the Demanova cave system (the Nízkie Tatry Mts., Slovakia). *Ann. Soc. Geol. Pol.*, **67**, 439–450.

Hercman, H., **Bella, P.**, **Gradziński, M.**, **Głazek, J.**, **Nowicki, T.** and **Sujka, G.** (2006) Results of the U-series dating of speleothems from the Demänová Cave System in 1995–2005. In: *Výskum využívanie a ochrana jaskýň, 5th Scientific Conference (Demänovská Dolina, 26–29. 9. 2005), Proceedings* (Ed. Bella, P.), pp. 26–35. SSJ, Liptovský Mikuláš. [In Slovak, with English abstract.].

Hercman, H., **Gąsiorowski, M.**, **Pawlak, J.**, **Błaszczyk, M.**, **Gradziński, M.**, **Matoušková, Š.**, **Zawidzki, P.** and **Bella, P.** (2020) Atmospheric circulation and the differentiation of precipitation sources during the Holocene inferred from five stalagmite records from Demänová Cave System (Central Europe). *Holocene*, **30**, 834–846.

Hercman, H., **Gradziński, M.** and **Bella, P.** (2008) Evolution of Brestovská Cave based on U–series dating of speleothems. *Geochronometria*, **32**, 1–12.

Herich, P. (2017) Demänová caves: The most extensive underground karst phenomenon in Slovakia. *Bull. Slov. Speleol. Soc.*, **2017**, 27–38.

Herman, E.K., **Toran, L.** and **White, W.B.** (2012) Clastic sediment transport and storage in fluviokarst aquifers: an essential component of karst hydrogeology. *Carbonates Evaporites*, **27**, 211–241.

Hochmuth, Z. (1993) Result of detailed mapping and additional geomorphological research of the Vyvieranie Cave in the Demänová Valley. *Slov. Kras*, **31**, 29–42. [In Slovak, with English summary.].

Hochmuth, Z. (1997) The correlation between the level of subterranean river beds and longitudinal profile of the valleys in allogenic karst explained on the examples of the Jánska and Demänová valleys. *Acta Fac. Stud. Human. Et Natur. Univer. Prešov. Prír. Vedy*, **28**, 103–121. [In Slovak, with English summary.].

Holden, N.E. (1990) Total half-lives for selected nuclides. *Pure Appl. Chem.*, **62**, 941–958.

Hók, J., **Kysel, R.**, **Kováč, M.**, **Moczo, P.**, **Kristek, J.**, **Kristeková, M.** and **Šujan, M.** (2016) A seismic source zone model for the seismic hazard assessment of Slovakia. *Geol. Carpath.*, **67**, 273–288.

Ivanovich, M. and **Harmon, R.S.** (1992) *Uranium Series Disequilibrium. Applications to Environmental Problems.* Clarendon, Oxford 571 pp.

Ivy-Ochs, S., **Schäfer, J.**, **Kubik, P.W.**, **Synal, H.-A.** and **Schlüchter, C.** (2004) Timing of deglaciation on the northern Alpine foreland (Switzerland). *Eclogae Geol. Helv.*, **97**, 47–55.

Jaffey, A.H., **Flynn, K.F.**, **Glendenin, L.E.**, **Bentley, W.C.** and **Essling, A.M.** (1971) Precision measurement of half-lives and specific activities of U-235 and U-238. *Phys. Rev. C*, **4**, 1889–1905.

Jankovská, V., **Chromý, P.** and **Nižnanská, M.** (2002) "Šafárka"– first palaeobotanical data of the character of Last Glacial vegetation and landscape on the West Carpathians (Slovakia). *Acta Palaeobot.*, **42**, 29–52.

Jankovská, V. and **Pokorný, P.** (2008) Forest vegetation of the last full–glacial period in the Western Carpathians (Slovakia and Czech Republic). *Preslia*, **80**, 307–324.

Jansen, J.D. (2006) Flood magnitude-frequency and lithologic control on bedrock river incision in post-orogenic terrain. *Geomorphology*, **82**, 39–57.

Jass, C.N. and **George, C.O.** (2010) An assessment of the contribution of fossil cave deposits to the Quaternary paleontological record. *Quatern. Inter.*, **217**, 105–116.

Jennings, J.N. (1985) *Karst Geomorphology*. Blackwell, New York, 293 pp.

Jopling, A.V. (1965) Hydraulic factors controlling the shape of laminae in laboratory deltas. *J. Sed. Petrol.*, **35**, 777–791.

Kadlec, J., **Chadima, M.**, **Lisa, L.**, **Hercman, H.**, **Osintsev, A.** and **Oberhaensli, H.** (2008) Clastic cave deposits in Botovskaya Cave (Eastern Siberia, Russian Federation). *J. Cave Karst Stud.*, **70**, 142–155.

Kagan, E.J., **Agnon, A.**, **Bar-Matthews, M.** and **Ayalon, A.** (2005) Dating large infrequent earthquakes by damaged cave deposits. *Geology*, **33**, 261–264.

Kicińska, D., **Hercman, H.** and **Najdek, K.** (2017) Evolution of the Bystrej Valley caves (Tatra Mts, Poland) based on corrosive forms, clastic deposits and U-series speleothem dating. *Ann. Soc. Geol. Pol.*, **87**, 101–119.

Knapp, E.P., **Terry, D.O.**, **Harbor, D.J.** and **Thren, R.C.** (2004) Reading Virginia's paleoclimate from the geochemistry and sedimentology of clastic cave sediments. In: *Studies of Cave Sediments: Physical and Chemical Records of Paleoclimate* (Eds Mylroie, J.E. and Sasowskyr, I.D.), pp. 95–106. Kluwer, New York.

Kojdová, M. and **Slíva, L.** (2005) Sedimentological characteristics of selected profiles of the Demänová Cave of Liberty. *Slov. Kras*, **43**, 129–144. [In Slovak, with English abstract.].

Kováč, M., **Bielik, M.**, **Kronome, B.**, **Moczo, P.**, **Sefara, J.** and **Sujan, M.** (2002) Seismic activity and neotectonic evolution of the Western Carpathians (Slovakia). *EGU Stephan Mueller Spec. Publ. Ser.*, **3**, 167–184.

Li, W.X., **Lundberg, J.**, **Dickin, A.P.**, **Ford, D.C.**, **Schwarcz, H.P.**, **McNutt, R.** and **Williams, D.** (1989) High-precision mass-spectrometric uranium-series dating of cave deposits and implications for palaeoclimate studies. *Nature*, **339**, 534.

Lindner, L. and **Marks, L.** (2015) Early and Middle Pleistocene fluvial series in northern foreland of the Carpathians (Poland and Ukraine) and their relation to Dnistr River terraces. *Quatern. Inter.*, **357**, 22–32.

Lisiecki, L.E. and **Raymo, M.E.** (2005) A Pliocene-Pleistocene stack of 57 globally distributed 907 benthic δ18O records. *Paleoceanography*, **20**, PA1003.

Louček, D., **Michovská, J.** and **Trefná, E.** (1960) Glaciation of the Low Tatra Mountains. *Sbor. Českoslov. Spol. Zem.*, **65**, 326–352. [In Czech with English summary.].

Luetscher, M. (2013) Glacial processes in caves. In: *Treatise on Geomorphology. Vol. 6, Karst Geomorphology* (Eds Shroder, J. and Frumkin, A.), pp. 258–266. Academic Press, San Diego, CA.

Makos, M., **Rinterknecht, V.**, **Braucher, R.**, **Tołoczko-Pasek, A.** and **Team, A.** (2018) Glacial Maximum and Lateglacial in the Polish High Tatra Mountains - Revised deglaciation chronology based on the 10Be exposure age dating. *Quatern. Sci. Rev.*, **187**, 130–156.

Marks, L. (2011) Quaternary Glaciations in Poland. *Develop. Quatern. Sci.*, **15**, 299–303.

Marks, L., **Dzierżek, J.**, **Janiszewski, R.**, **Kaczorowski, J.**, **Lindner, L.**, **Majecka, A.**, **Makos, M.**, **Szymanek, M.**, **Tołoczko-Pasek, A.** and **Woronko, B.** (2016) Quaternary stratigraphy and palaeogeography of Poland. *Acta Geol. Pol.*, **66**, 403–427.

Marks, L., **Bińka, K.**, **Woronko, B.**, **Majecka, A.** and **Teodorski, A.** (2019) Revision of the late Middle Pleistocene stratigraphy and palaeoclimate in Poland. *Quatern. Intern.*, **534**, 5–17.

Martelli, L., **Boncio, P.**, **Baglione, M.**, **Cavuoto, G.**, **Mancini, M.**, **Scarascia Mugnozza, G.** and **Tallini, M.** (2012) Main geologic factors controlling site response during the 2009 L'Aquila earthquake. *Ital. J. Geosci.*, **131**, 423–439.

Martini, I. (2011) Cave clastic sediments and implications for speleogenesis: new insights from the Mugnano Cave (Montagnola Senese, Northern Apennines, Italy). *Geomorphology*, **134**, 452–460.

Martini, I., **Ronchitelli, A.**, **Arrighi, S.**, **Capecchi, G.**, **Ricci, S.**, **Scaramucci, S.**, **Gambassini, P.** and **Moroni, A.** (2018) Cave clastic sediments as a tool for refining the study of human occupation of prehistoric sites: insights from the cave site of La Cala (Cilento, southern Italy). *J. Quatern. Sci.*, **33**, 586–596.

Molodkov, A. (2001) ESR dating evidence for early man at a Lower Palaeolithic cave-site in the Northern Caucasus as derived from terrestrial mollusc shells. *Quatern. Sci. Rev.*, **20**, 1051–1055.

Moseley, G.E., **Spötl, C.**, **Svensson, A.**, **Cheng, H.**, **Brandstätter, S.** and **Edwards, R.L.** (2014) Multi-speleothem record reveals tightly coupled climate between central Europe and Greenland during Marine Isotope Stage 3. *Geology*, **42**, 1043–1046.

Moseley, G.E., **Spötl, C.**, **Cheng, H.**, **Boch, R.**, **Min, A.** and **Edwards, R.L.** (2015) Termination-II interstadial/stadial

climate change recorded in two stalagmites from the north European Alps. *Quatern. Sci. Rev.*, **127**, 229–239.

Motyka, J., Gradziński, M., Bella, P. and Holúbek, P. (2005) Chemistry of waters from selected caves in Slovakia – a reconnaissance study. *Environ. Geol.*, **48**, 682–692.

NACSN (North American Commission on Stratigraphic Nomenclature) (1983) North American stratigraphic code. *AAPG Bull.*, **67**, 841–875.

Nanson, G.C. and Huang, H.Q. (2017) Self-adjustment in rivers: Evidence for least action as the primary control of alluvial-channel form and process. *Earth Surf. Process. Landforms*, **42**, 575–594.

Nicholas, A.P., Aalto, R.E., Sambrook Smith, G.H. and Schwendel, A.C. (2018) Hydrodynamic controls on alluvial ridge construction and avulsion likelihood in meandering river floodplains. *Geology*, **46**, 639–642.

Obu, J., Košutnik, J., Overduin, P.P., Boike, J., Blatnik, M., Zwieback, S., Gostinčar, P. and Mihevc, A. (2018) Sorted patterned ground in a karst cave, Ledenica pod Hrušico, Slovenia. *Permafrost Periglac. Process.*, **29**, 121–130.

Oliveira, E.V., Villa Nova, P., Goin, F.J. and Avilla, L.S. (2011) A new hyaladelphine marsupial (Didelphimorphia, Didelphidae) from cave deposits of northern Brazil. *Zootaxa*, **3041**, 51–62.

Orvošová, M., Deininger, M. and Milovský, R. (2014) Permafrost occurrence during the Last Permafrost Maximum in the Western Carpathian Mountains of Slovakia as inferred from cryogenic cave carbonate. *Boreas*, **43**, 750–758.

Palmer, A.N. (2007) *Cave Geology*. Cave Books, Dayton, 454 pp.

Pickering, R., Hancox, P.J., Lee-Thorp, J.A., Grün, R., Mortimer, G.E., McCulloch, M. and Berger, L.R. (2007) Stratigraphy, U-Th chronology, and paleoenvironments at Gladysvale Cave: insights into the climatic control of South African hominin-bearing cave deposits. *J. Human Evol.*, **53**, 602–619.

Pickering, R., Kramers, J.D., Hancox, P.J., de Ruiter, D.J. and Woodhead, J.D. (2011) Contemporary flowstone development links early hominin bearing cave deposits in South Africa. *Earth Planet. Sci. Lett.*, **306**, 23–32.

Podgórska, D. (2019) Reconstruction of Vistulian palaeoenvironmental conditions based on analysis of speleothems from the Demänová Cave System. Unpubl. PhD thesis, Jagiellonian University, Kraków, 116 pp.

Polyak, V.J., Onac, B.P., Fornós, J.J., Hay, C., Asmerom, Y., Dorale, J.A., Ginés, J., Tuccimei, P. and Ginés, A. (2018) A highly resolved record of relative sea level in the western Mediterranean Sea during the last interglacial period. *Nature Geosci.*, **11**, 860–864.

Quinif, Y. and Maire, R. (1998) Pleistocene deposits in Pierre Saint-Martin Cave, French Pyrenees. *Quatern. Res.*, **49**, 37–50.

Richards, K.S. (1982) *Rivers: Form and Process in Alluvial Channels*. Methuen, London, 358 pp.

Sasowsky, I. (2007) Clastic sediments in caves – imperfect recorders of processes in karst. *Acta Carsol.*, **36**, 143–149.

Schlüchter, C. (2008) The ice age in the Alps. In: *The Geology of Central Europe* (Ed. McCann, T.), vol. **2**, pp. 1304–1310. The Geological Society, London.

Schumm, S.A. (1985) Patterns of alluvial rivers. *Annu. Rev. Earth Planet. Sci.*, **13**, 5–27.

Shang, H., Tong, H., Zhang, S., Chen, F. and Trinkaus, E. (2007) An early modern human from Tianyuan Cave, Zhoukoudian, China. *Proc. China Nat. Acad. Sci.*, **104**, 6573–6578.

Spötl, C. and Mangini, A. (2007) Speleothems and palaeoglaciers. *Earth Planet. Sci. Lett.*, **254**, 323–331.

Spötl, C., Mangini, A., Frank, N., Eichstädter, R. and Burns, S.J. (2002) Start of the last interglacial period at 135 ka: evidence from a high Alpine speleothem. *Geology*, **30**, 815–818.

Spötl, C., Scholz, D. and Mangini, A. (2008) A terrestrial U/Th-dated stable isotope record of the Penultimate Interglacial. *Earth Planet. Sci. Lett.*, **276**, 283–292.

Stein, J.K. (1987) Deposits for archaeologists. In: *Advances in Archaeological Method and Theory* (Ed. Schiffer, M.B.), **7**, 337–395. Academic Press, New York.

Sweeting, M.J. (1973) *Karst Landforms*. Columbia University Press, New York, 362 pp.

Szczygieł, J. (2015) Quaternary faulting in the Tatra Mountains, evidence from cave morphology and fault-slip analysis. *Geol. Carpath.*, **66**, 245–254.

Szczygieł, J., Mendecki, M., Hercman, H., Wróblewski, W. and Glazer, M. (2019) Relict landslide development as inferred from speleothem deformation, tectonic data, and geoelectrics. *Geomorphology*, **330**, 116–128.

Tinkler, K.J. and Wohl, E.E. (Eds) (1998) Rivers over rock: Fluvial processes in bedrock channels. *AGU Geophys. Monogr.*, **107**, 323.

Tooth, S., Brandt, D., Hancox, P.J. and McCarthy, T.S. (2004) Geological controls on alluvial river behaviour: a comparative study of three rivers on the South African Highveld. *J. Afr. Earth Sci.*, **38**, 79–97.

Vitásek, F. (1923) Studie pleistocenu v údolí Demänovky. *Sbor. Stát. Geol. Úst. Českosl. Rep.*, **2**, 157–171. [In Slovak.].

Warwick, G.T. (1976) Geomorphology and caves. In: *The Science of Speleology* (Eds Ford, T.D. and Cullingford, C.H.D.), pp. 61–125. Academic Press, London.

Whipple, K.X., Dibiase, R.A. and Crosby, B.T. (2013) Bedrock rivers. In: *Treatise on Geomorphology* (Ed. Shroder, J.), vol. **9**, pp. 550–573. Elsevier, Amsterdam.

White, E.L. and White, W.B. (1968) Dynamics of sediment transport in limestone caves. *Nat. Speleol. Soc. Bull.*, **30**, 115–129.

White, W.B. (2007) Cave sediments and paleoclimate. *J. Cave Karst Stud.*, **69**, 76–93.

Wiejacz, P. and Dębski, W. (2009) Podhale, Poland, earthquake of November 30, 2004. *Acta Geophys.*, **57**, 346–366.

Wirsig, C., Zasadni, J., Christl, M., Akçar, N. and Ivy-Ochs, S. (2016) Dating the onset of LGM ice surface lowering in the High Alps. *Quatern. Sci. Rev.*, **143**, 37–50.

Wright, L.D. (1977) Sediment transport and deposition at river mouths: a synthesis. *Geol. Soc. Am. Bull.*, **88**, 857–868.

Wu, X., Zhang, C., Goldberg, P., Cohen, D., Pan, Y., Arpin, T. and Bar-Yosef, O. (2012) Early pottery at 20,000 years ago in Xianrendong Cave, China. *Science*, **336**, 1696–1700.

Yonge, C.J., Ford, D., Horne, G., Lauriol, B. and Schroeder, J. (2018) Ice caves in Canada. In: *Ice Caves* (Eds Perşoiu, A. and Lauritzen, S.-E.), pp. 285–334. Elsevier, Amsterdam.

Zupan Hajna, N., Mihević, A., Pruner, P. and Bosák, P. (2008) Palaeomagnetism and Magnetostratigraphy of Karst Sediments in Slovenia. *Carsologica*, **8**, 266.